Proteomic and Biochemical Studies of Lysine Malonylation Suggest Its Malonic Aciduria-associated Regulatory Role in Mitochondrial Function and Fatty Acid Oxidation*[S]

Gozde Colak,[a,b] Olga Pougovkina,[b,c] Lunzhi Dai,[a,b] Minjia Tan,[d,e] Heleen te Brinke,[c] He Huang,[a] Zhongyi Cheng,[f] Jeongsoon Park,[g] Xuelian Wan,[d] Xiaojing Liu,[h] Wyatt W. Yue,[i] Ronald J. A. Wanders,[c,j] Jason W. Locasale,[h] David B. Lombard,[g] Vincent C. J. de Boer,[c,j,k] and Yingming Zhao[a,d,l]

The protein substrates of sirtuin 5-regulated lysine malonylation (Kmal) remain unknown, hindering its functional analysis. In this study, we carried out proteomic screening, which identified 4042 Kmal sites on 1426 proteins in mouse liver and 4943 Kmal sites on 1822 proteins in human fibroblasts. Increased malonyl-CoA levels in malonyl-CoA decarboxylase (MCD)-deficient cells induces Kmal levels in substrate proteins. We identified 461 Kmal sites showing more than a 2-fold increase in response to MCD deficiency as well as 1452 Kmal sites detected only in MCD−/− fibroblast but not MCD+/+ cells, suggesting a pathogenic role of Kmal in MCD deficiency. Cells with increased lysine malonylation displayed impaired mitochondrial function and fatty acid oxidation, suggesting that lysine malonylation plays a role in pathophysiology of malonic aciduria. Our study establishes an association between Kmal and a genetic disease and offers a rich resource for elucidating the contribution of the Kmal pathway and malonyl-CoA to cellular physiology and human diseases. ***Molecular & Cellular Proteomics 14: 10.1074/mcp.M115.048850, 3056–3071, 2015.***

Reversible acetylation at lysine residues in proteins has been extensively studied over the past few decades (1, 2). This modification is now known to have important regulatory roles in diverse cellular processes and physiological conditions, such as transcription, metabolism, and aging (3–5). Dysregulation of the lysine acetylation pathway is associated with various diseases, such as cardiovascular disease and cancer (6, 7). In addition to acetylation, recent studies show that lysine residues in proteins can be modified by a family of short-chain acylations: propionylation, butyrylation, crotonylation, malonylation, succinylation, glutarylation, and 2-hydroxyisobutyrylation (8–13). Notable among the seven types of new lysine acylation pathways are lysine malonylation (Kmal),[1] succinylation (Ksucc), and glutarylation (Kglu). Each of the three types of modifications have an acidic carboxylic group that changes the charge status from +1 to −1 charge at physiological pH, which is similar to that caused by protein phosphorylation but more significant than lysine acetylation (Fig. 1*A*). Accordingly, these acidic lysine acylations likely have a more substantial impact on the substrate protein's structure and function than lysine acetylation when modified at the same lysine residue(s). Recent studies demonstrate that pyruvate dehydrogenase complex, succinate dehydrogenase,

From the [a]Ben May Department of Cancer Research, University of Chicago, Chicago, Illinois 60637, [c]Laboratory of Genetic Metabolic Diseases, Department of Clinical Chemistry and [j]Department of Pediatrics, Emma's Children Hospital, Academic Medical Center, University of Amsterdam, Meibergdreef 9, 1105 AZ Amsterdam, The Netherlands, [d]State Key Laboratory of Drug Research, Shanghai Institute of Materia Medica, Chinese Academy of Sciences, Shanghai 201203, China, [f]PTM Biolabs, Chicago, Illinois 60612, [g]Department of Pathology and Institute of Gerontology, University of Michigan, Ann Arbor, Michigan 48109, [h]Division of Nutritional Sciences, Cornell University, Ithaca, New York 14853, and [i]Structural Genomics Consortium, University of Oxford, Oxford OX3 7DQ, United Kingdom

Received, February 6, 2015, and in revised form, August 14, 2015
Published, MCP Papers in Press, August 28, 2015, DOI 10.1074/mcp.M115.048850

Author contributions: G. C., M. T., V. C. J. d. B., and Y. Z. designed research; G. C., O. P., L. D., M. T., H. t. B., H. H., J. P., X. L., W. W. Y., J. W. L., D. B. L., and V. C. J. d. B. performed research; O. P., L. D., M. T., H. t. B., H. H., Z. C., J. P., X. L., W. W. Y., R. J. A. W., J. W. L., D. B. L., and V. C. J. d. B. contributed new reagents or analytic tools; G. C., O. P., M. T., H. H., X. W., X. L., J. W. L., V. C. J. d. B., and Y. Z. analyzed data; G. C., M. T., H. H., and Y. Z. wrote the paper.

[1] The abbreviations used are: Kmal, lysine malonylation; CPT, carnitine palmitoyltransferase; GO, gene ontology; Kac, lysine acetylation; Ksucc, lysine succinylation; Kglu, lysine glutarylation; MCD, malonyl-CoA decarboxylase; MCD+/+, MCD wild type; MCD−/−, MCD-deficient; PTM, post-translational modification; KO, knock-out; SILAC, stable isotope labeling by amino acids in cell culture; SIRT, sirtuin; OCR, oxygen consumption rate; VLCAD, very long-chain acyl-CoA dehydrogenase; LCHAD, long-chain 3-hydroxyacyl-CoA dehydrogenase; KEGG, Kyoto Encyclopedia of Genes and Genomes; adj, adjusted.

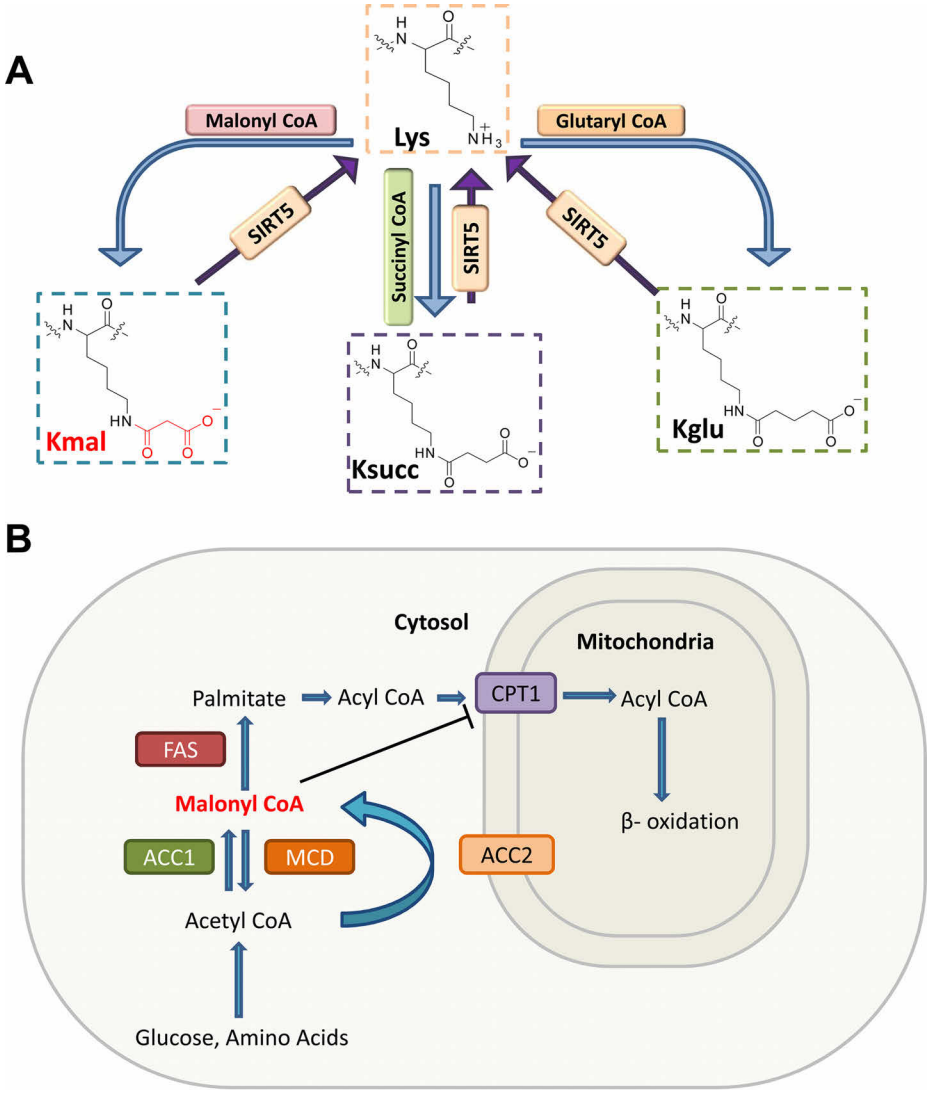

FIG. 1. **Lysine malonylation and biosynthesis of malonyl-CoA.** *A*, structures of malonyllysine (*Kmal*), succinyllysine (*Ksucc*), and glutaryllysine (*Kglu*). SIRT5 is an enzyme with demalonylation, desuccinylation, and deglutarylation activities. *B*, illustration of malonyl-CoA metabolism. *FAS*, fatty-acid synthase; *ACC1* and *ACC2*, acetyl-CoA carboxylases 1 and 2.

and carbamoyl-phosphate synthase 1 can be regulated by Ksucc and Kglu, respectively, suggesting that acidic lysine acylation pathways can have unique functions distinct from the widely studied lysine acetylation pathway (10, 11).

Kmal was initially identified in both *Escherichia coli* and mammalian cells by using HPLC-MS/MS, co-elution of synthetic peptides, isotopic labeling, and Western blotting analysis with pan anti-Kmal antibodies (8, 15). Lin and co-workers (9) and our group (10, 11, 15) have previously demonstrated robust enzymatic activities of SIRT5, both *in vitro* and *in vivo*, in demalonylation, desuccinylation, and deglutarylation. The demalonylation and desuccinylation activities of SIRT5 require NAD^+ but can be inhibited by nicotinamide, a class III histone deacetylase inhibitor (15). Given the fact that isotopic malonate can label lysine malonylation and that acyl-CoAs are the precursor for other lysine acylations (*e.g.* acetyl-CoA for lysine acetylation), malonyl-CoA is likely the precursor for the lysine malonylation reaction (8, 15). Despite this progress, the substrates for this new modification pathway remain largely unknown, representing a major bottleneck for studying its biological functions.

Malonyl-CoA is a tightly regulated metabolic intermediate in mammalian cells (16). Malonyl-CoA is produced by acetyl-CoA carboxylase and consumed by malonyl-CoA decarboxylase (MCD; EC 4.1.1.9), fatty-acid synthase, and fatty acid elongases (16) (Fig. 1*B*). In addition to being a key intermediate for fatty acid biosynthesis and fatty acid elongation, malonyl-CoA has diverse regulatory functions. Malonyl-CoA was shown to be a potent inhibitor of carnitine palmitoyltransferase 1 (CPT1) and thereby regulates hepatic fatty acid synthesis, β-oxidation, and ketogenesis (16) (Fig. 1*B*). It was reported that malonyl-CoA can function as a key intermediate in the hypothalamus as an energy sensor (17). Higher malonyl-CoA levels are observed in skeletal muscle biopsies of type 2 diabetic patients (18). Elevated fatty acid oxidation observed during cardiac ischemia/reperfusion has been attributed to the reduction of malonyl-CoA levels in the heart. Accordingly, increasing malonyl-CoA levels has been proposed as a strat-

egy to improve cardiac function (19). Acetyl-CoA carboxylases, enzymes that are known to be important for biosynthesis of malonyl-CoA, are associated with physiology and diseases. Mice with genetic knock-out of acetyl-CoA carboxylase 2 gene are resistant to obesity and diabetes when fed with high calorie diets (20). Accordingly, acetyl-CoA carboxylases have been proposed as drug targets for diverse human diseases including diabetes, obesity, and cancer (21). Nevertheless, potential roles for malonyl-CoA in human pathology are not well understood.

MCD is a 55-kDa enzyme that catalyzes conversion of malonyl-CoA to acetyl-CoA, thus maintaining homeostatic levels of these metabolites in mitochondria and peroxisomes. In the cytosol, malonyl-CoA is controlled by two enzymes with opposite activities, MCD and acetyl-CoA carboxylase. MCD deficiency, or malonic aciduria, is an inborn metabolic disorder caused by MCD mutations that reduce or eliminate activity of this enzyme and therefore compromise conversion of malonyl-CoA to acetyl-CoA (22). These patients have high levels of malonylcarnitine in blood and high level of organic acids, such as malonic acid, in the urine (23). Diverse symptoms are observed among malonic aciduria patients including delayed development, seizures, diarrhea, vomiting, low blood sugar (hypoglycemia), and cardiomyopathy (22). It appears that inhibition of fatty acid catabolism caused by a high level of malonyl-CoA is at least partially responsible for the manifestations of disease. We recently showed that MCD-deficient (MCD−/−) patient cells show increased Kmal levels (24). Therefore it is possible that Kmal could be an important mechanism mediating the pathophysiology of MCD deficiency. Nevertheless, how the increased Kmal levels, caused by a high level of malonic acid in malonic aciduria patients and other diseases, impacts cellular function and regulates physiology remains unknown.

In this study, we used a proteomics approach to identify Kmal substrates and map their modification sites by affinity enrichment of malonylated peptides and HPLC-MS/MS analysis. We identified 4016 Kmal sites on 1395 proteins in *Sirt5* knock-out mouse liver and 4943 Kmal peptides on 1831 proteins in MCD+/+ and MCD−/− human fibroblasts. Four hundred sixty-one Kmal sites on 339 proteins showed a 2-fold or greater increase in MCD−/− cells relative to MCD+/+ cells, and 1452 Kmal sites on 822 proteins were only detected in MCD−/− cells, suggesting that MCD activity has a profound impact on Kmal levels and distribution. The malonylated proteins induced in MCD−/− cells are associated with diverse pathways including fatty acid metabolism and neurological diseases. We further showed that MCD−/− cells with increased lysine malonylation have impaired mitochondrial respiration and fatty acid oxidation. Our proteomics data illuminate the landscape of the Kmal modification in mammalian cells, offer a valuable resource for studying its biology, and propose possible roles of Kmal in diseases associated with dysregulation of malonyl-CoA homeostasis.

EXPERIMENTAL PROCEDURES

Materials—Chemicals were purchased as analytical grade from Sigma-Aldrich, Inc. (St. Louis, MO). Modified sequencing grade trypsin was purchased from Promega Corp. (Madison, WI). Pan-anti-malonyllysine antibody and pan-anti-malonyllysine-agarose beads were from PTM Biolabs, Inc. (Chicago, IL). MS grade water and acetonitrile were from Thermo Fisher Scientific (Waltham, MA). C_{18} ZipTips were purchased from Millipore Corp. (Billerica, MA). SILAC DMEM (CCFDA003-132J01) was purchased from UCSF Cell Culture Facility (San Francisco, CA). XerumFree reagent (XF205) was purchased from MayFlower Bioscience (St. Louis, MO). Dialyzed serum (Gibco 26400) was purchased from Life Technologies, Thermo Fisher Scientific.

Preparation of Mouse Liver Lysate—Four two-month-old male *Sirt5* KO mice (25, 26) were anesthetized with an isoflurane overdose, and the blood in the liver was removed by perfusion with ice-cold PBS for 5 min. Liver was homogenized in a glass Dounce homogenizer in SDS lysis buffer (20 mM Tris-HCl, pH 6.8, 1% SDS, 5% β-mercaptoethanol, 10% glycerol, 25 mM nicotinamide). The lysates from four livers were pooled together, and the sample was clarified by centrifugation at 16,000 × *g*. The protein in the supernatant was precipitated with 10% (v/v) trichloroacetic acid. Then the precipitated proteins were in solution-digested with trypsin as described previously (27).

Preparation of SILAC Samples—Human dermal fibroblast cells lines MCD+/+ (control cells) and MCD−/− cells were obtained from Gaslini Biobank, Italy. The cells were grown in SILAC DMEM supplemented with L-glutamine (584 mg/liter), 10% (v/v) dialyzed serum, and 2% (v/v) serum-free reagent. Regular L-lysine ($^{12}C_6$,$^{14}N_2$-labeled) and L-arginine ($^{12}C_6$,$^{14}N_2$-labeled) were added to the "light" medium (final concentration, 100 mg/liter) used for culturing MCD−/− cells. "Heavy" isotopic L-lysine ($^{13}C_6$,$^{15}N_2$-labeled) and light L-arginine ($^{12}C_6$,$^{14}N_2$-labeled) were added to the heavy medium (final concentration, 100 mg/liter) used for culturing MCD+/+ control cells. Both cell lines were grown in parallel until MCD+/+ cells were sufficiently labeled by the isotopic lysine.

Both MCD+/+ and MCD−/− cells were lysed in SDS buffer (20 mM Tris-HCl, pH 6.8, 1% SDS, 5% β-mercaptoethanol, 10% glycerol, 25 mM nicotinamide). Twelve milligrams of each cell lysate were mixed and precipitated overnight by 10% TCA for tryptic digestion.

HPLC Fractionation—The tryptic peptides were fractionated by using a reversed phase column (Luna C_{18}, 10 × 250 mm, 5-μm particle, 100-Å pore size, Phenomenex Inc., Torrance, CA) in a Discovery VP preparative HPLC system (Shimadzu Corp., Kyoto, Japan). The peptides were fractionated into 75 fractions using a gradient from 2 to 90% buffer B (10 mM ammonium formate in 90% acetonitrile and 10% water, pH 7.8) in buffer A (10 mM ammonium formate in water, pH 7.8) at a flow rate of 4 ml/min in 60 min. The 75 fractions were finally combined equally into five final fractions for mouse liver samples and 10 final fractions for MCD SILAC samples, respectively. Each fraction was condensed by using a SpeedVac (ThermoSavant SPD111V). The peptide solution was used for immunoaffinity enrichment.

Affinity Enrichment of the Peptides Containing Kmal—The peptides containing Kmal were enriched using a procedure described previously (27). The tryptic peptides from each fraction were resolubilized in 100 mM NH_4HCO_3, pH 8.0. Samples were centrifuged at 20,000 × *g* for 10 min to remove insoluble particles. The peptides were incubated with 15 μl of agarose beads conjugated with anti-malonyllysine antibody at room temperature for 4 h with gentle rotation. The beads were washed three times with NETN buffer (50 mM Tris-HCl, pH 8.0, 100 mM NaCl, 1 mM EDTA, 0.5% Nonidet P-40), twice with ETN buffer (50 mM Tris-HCl, pH 8.0, 100 mM NaCl, 1 mM EDTA), and once with water. Enriched Kmal peptides were eluted from the beads by wash-

ing three times with 0.1% trifluoroacetic acid. The eluted Kmal peptides were dried in a SpeedVac.

Nano-HPLC-MS/MS Analysis—The enriched Kmal samples were first desalted using OMIX C_{18} tips (Agilent Technologies Inc., Santa Clara, CA) and then dissolved in solvent A (0.1% formic acid in water). Samples were injected onto a manually packed reversed phase C_{18} column (100 mm × 75 μm, 3-μm particle size, Dr. Maisch GmbH, Ammerbuch, Germany) connected to an Easy-nLC 1000 HPLC system (Thermo Fisher Scientific Inc., Waltham, MA). Peptides were eluted from 5 to 90% solvent B (0.1% formic acid and 1% water in acetonitrile) in solvent A with a 1-h gradient at a flow rate of 200 nl/min. The analytes were directly ionized and sprayed into a Q Exactive mass spectrometer (Thermo Fisher Scientific Inc.) by Nanospray Flex™ Ion Sources. Full MS scans were acquired in the Orbitrap mass analyzer over the range *m/z* 300–1400 with a mass resolution of 70,000 at *m/z* 200. The 15 most intense peaks of the precursor ions were fragmented in the high energy collision dissociation collision cell with normalized collision energy of 27, and tandem mass spectra were acquired with a mass resolution of 17,500 at *m/z* 200. Lock mass at *m/z* 445.120024 was enabled for internal calibration of the full MS spectrum. Ions with either a single charge or more than four charges were excluded from MS/MS fragmentation, and the dynamic exclusion duration was set to 25 s.

Data Processing and Analysis—MaxQuant software (version 1.3.0.5) was used for identifying and quantifying protein and malonylated peptides. Peak list generation and precursor mass recalibration of the raw MS data were carried out by MaxQuant software. Trypsin was specified as the cleavage enzyme, and the maximum number of missed cleavage was set at 3. Methionine oxidation, protein N-terminal acetylation, lysine acetylation (Kac), Kmal (specified for neutral loss of CO_2 in MS/MS fragmentation), and Ksucc were specified as variable modifications, and cysteine alkylation by iodoacetamide was specified as a fixed modification for all database searching. Database searching was performed against the UniProt mouse (50,807 sequences; release date, May 2013) or human (88,817 sequences; release date, February 2014) reference protein sequence database concatenated with a reversed decoy database with initial precursor mass tolerance of 7 ppm. Mass tolerance for fragment ions was set at 20 ppm. False discovery rate thresholds for protein, peptide, and modification site were fixed at 0.01. The identified peptides with MaxQuant Andromeda score below 50 and localization probability below 0.75 were removed prior to bioinformatics analysis.

Malonyl-CoA Measurement—The cells were treated with 15 μM orlistat or vehicle only for 24 h at 80% confluence. The media were quickly removed, and the dishes were placed on top of dry ice. One milliliter of extraction solvent (80% methanol in water) was immediately added, and the dishes were transferred to the −80 °C freezer. The dishes were left for 15 min, and then cells were scraped into extraction solvent on dry ice. The whole solution was centrifuged at 20,000 × *g* at 4 °C for 10 min. Cell extracts were prepared from 3 wells to make biological triplicates. The supernatant from the tissue extract was transferred to a new tube for LC-MS/MS analysis. All samples were dried in a vacuum concentrator (SpeedVac, Thermo Fisher Scientific Inc.).

An Ultimate 3000 UHPLC (Thermo Fisher Scientific Inc.) was coupled to Q Exactive mass spectrometer (Thermo Fisher Scientific Inc.) for metabolite separation and detection. For acyl-CoA analysis, a reversed phase LC method was used. A Luna C_{18} column (100 × 2.0-mm inner diameter, 3 μm, Phenomenex Inc.) was used with mobile phase A (water with 5 mM ammonium acetate, pH 6.8) and mobile phase B (methanol) at a flow rate of 0.2 ml/min. The linear gradient was as follows: 0 min, 2% B; 1.5 min, 2% B; 3 min, 15% B; 5.5 min, 95% B; 14.5 min, 95% B; 15 min, 2% B; 20 min, 2% B. The column was at room temperature.

The Q Exactive mass spectrometer was equipped with an heated ESI probe, and the relevant parameters were as follows: heater temperature, 120 °C; sheath gas, 30; auxiliary gas, 10; sweep gas, 3; spray voltage, 3.6 kV for positive mode. The capillary temperature was set at 320 °C, and S-lens was 55. A full scan range was set at 300–1000 (*m/z*). The resolution was set at 70,000 (at *m/z* 200). The maximum injection time was 200 ms. Automated gain control was targeted at 3×10^6 ions. For CoA analysis, cell extract was dissolved into 30 μl of water with 50 mM ammonium acetate, pH 6.8. Samples were centrifuged at 20,000 × g at 4 °C for 3 min, and the supernatant was transferred to LC vials. The injection volume was 8 μl for CoA analysis.

Raw data collected from LC-MS/MS were processed on Thermo Scientific software Sieve 2.0. Peak alignment and detection were performed according to the manufacturer's protocols. For a targeted metabolomics analysis, a frame seed including Acyl-CoA metabolites that was previously validated was used for targeted metabolite analysis with data collected in positive mode with the *m/z* width set at 8 ppm. Statistical significance was calculated based on Student's *t* test (unpaired, two-tailed).

Motif Analysis for Lysine Malonylation Substrates—The standalone version of iceLogo (version 1.2) software was used to analyze the preference of flanking Kmal site sequence from mouse liver or human MCD cells (28). The embedded Swiss-Prot "*Mus musculus*" or "*Homo sapiens*" was used as the negative set. Six flanking amino acid residues on each side of a lysine malonylated site were selected as the positive set.

Functional Enrichment Analysis—Functional enrichment analysis of lysine malonylated proteins was carried out using DAVID (Functional Annotation Bioinformatics Microarray Analysis) Bioinformatics Resources version 6.7 with the total mouse or human genome information as the background (29). All identified lysine malonylated proteins were subjected to database analyses using gene ontology (GO) (30) and Kyoto Encyclopedia of Genes and Genomes (KEGG) metabolic pathways (31). The GO Fat database from DAVID was selected in this analysis. The family-wide false discovery rate was corrected by the Benjamini-Hochberg method using an adjusted *p* value cutoff of 0.05.

Protein-Protein Interaction Network Analysis—Protein-protein interaction networks of the lysine malonylome were analyzed using the Search Tool for the Retrieval of Interacting Genes/Proteins (STRING) database (version 9.1; confidence score, 0.7) visualized by Cytoscape software (version 3.1.0) with the MCODE App toolkit (32). The confidence score is the approximate probability that a predicted link exists between two enzymes in the same metabolic map in the KEGG database. Confidence limits are as follows: low confidence, 0.2 (or better); medium confidence, 0.5; high confidence, 0.75; the highest confidence, 0.95.

Protein Complex Enrichment Analysis—Manually curated core complexes indexed by the CORUM (the comprehensive resource of mammalian protein complexes) database were used for the analysis of lysine malonylated substrates. Mouse or human complexes indexed in the database were used for enrichment analysis of mouse liver or MCD human cells by Fisher's exact test. Complexes with an adjusted *p* value <0.01 were considered as significant.

Kmal Stoichiometry Calculation—Absolute stoichiometry calculation of malonylated site in SILAC samples was based on the previously reported algorithm (33) with slight modification (34). The calculation was based on the MS quantification data (SILAC ratio) of the Kmal peptides (*x*), the corresponding protein (*z*), and the corresponding unmodified peptide (*y*) with the assumption that only one type of PTM occurs at a given site. The SILAC ratios of unmodified peptides (*y*) and proteins (*z*) were calculated from the global protein expres-

sion analysis using the whole cell lysate mixture of SILAC labeled MCD+/+ and MCD−/− cells without antibody affinity enrichment. The calculation assumed that only one type of PTM occurred at the given site of interest. The unmodified peptide was defined as the longest completely digested part of the peptide sequence derived from the malonylated peptide, which contains no other PTM. The absolute stoichiometry was calculated based on the SILAC ratios of *x*, *y*, and *z* using the same formula as reported previously (33).

Mitochondrial Respiratory Flux Analysis—Measurements of cellular oxygen consumption were performed using an extracellular flux analyzer (Seahorse BioScience, Billerica, MA). Fao hepatoma cells were incubated for 24 h in culture medium (DMEM supplemented with 2 mM HEPES, 2% penicillin/streptomycin, and 10% FBS) containing 50 mM malonate. Next, cells were plated at 20,000 cells/well in Seahorse 96-well culture plates followed by overnight incubation in malonate-free medium. Human fibroblasts were maintained and plated in DMEM supplemented with 2 mM HEPES, 2% penicillin/streptomycin, and 10% FBS at 30,000 cells/well. Seahorse mitochondrial function analysis was performed using the digitonin cell permeabilization protocol (35). Prior to measurements of respiration, culture medium was replaced with MAS buffer (pH 7.4, 220 mM mannitol, 70 mM sucrose, 10 mM KH_2PO_4, 5 mM $MgCl_2$, 2 mM HEPES, 1 mM EGTA, 0.6% fatty-acid free BSA). Oxygen consumption rate (OCR) was analyzed following a single injection of either pyruvate/malate/ADP/digitonin, succinate/rotenone/ADP/digitonin, or octanoylcarnitine/malate/ADP/digitonin dissolved in MAS buffer without BSA at pH 7.4. Final digitonin concentration was 30 μg/ml for Fao hepatoma cells and 100 μg/ml for fibroblasts. Final substrate concentrations were as follows: pyruvate, 5 mM; malate, 2.5 mM; succinate, 10 mM; octanoylcarnitine, 100 μM; ADP, 1 mM. After injection of substrate, oligomycin was injected at 1.5 μM final concentration followed by injection of antimycin (2.5 μM) and rotenone (1.25 μM).

Very Long-chain Acyl-CoA Dehydrogenase (VLCAD) Activity Analysis—VLCAD activity was analyzed by monitoring the specific conversion of palmitoyl-CoA (C16:0-CoA) into palmitenoyl-CoA (C16:1-CoA) in cell lysates (36). Cell lysates (0.1 mg/ml) were incubated in 0.125 mM Tris, pH 8.0, with 0.4 mM ferrocenium and 0.25 mM palmitoyl-CoA for 10 min at 37 °C, and the reaction was stopped by addition of 10 μl of 2 N HCl followed by neutralization with 10 μl of 2 M KOH, 0.6 M MES. Samples were deproteinated with acetonitrile followed by separation of substrate and products by reversed phase C_{18} HPLC and UV detection.

Long-chain 3-Hydroxyacyl-CoA Dehydrogenase (LCHAD) Activity Analysis—LCHAD activity was analyzed by incubating cell lysates (0.1 mg/ml) with 3-ketopalmitoyl-CoA (0.26 mM; synthesized in house) and 0.4 mM NADH in 100 mM MES, 200 mM potassium phosphate buffer with 0.1% Triton X-100, pH 6.2, for 5 min at 37 °C using a procedure described previously (37). To control for the conversion of 3-ketopalmitoyl-CoA by short-chain 3-hydroxyacyl-CoA dehydrogenase, samples were incubated with and without *N*-ethylmaleimide because *N*-ethylmaleimide inhibits only LCHAD and not short-chain 3-hydroxyacyl-CoA dehydrogenase. After incubation, reactions were stopped with 10 μl of 2 N HCL followed by neutralization with 10 μl of 2 M KOH, 0.6 M MES. Samples were deproteinated with acetonitrile followed by separation of substrate and products by reversed phase C_{18} HPLC and UV detection.

Immunocytochemistry—MCD+/+ and MCD−/− cells were grown on coverslips and treated with 15 μM orlistat for 48 h. MitoTracker Red was added to the culture medium at 0.1 μM final concentration and incubated for 30 min. The cells were washed with PBS twice, fixed with 4% (v/v) paraformaldehyde, and permeabilized with 0.2% (v/v) Triton X-100. The cells were blocked with 2% bovine serum albumin for 2 h and incubated with the corresponding primary antibodies at 1.5 μg/ml final concentration overnight. The cells were washed with PBS twice, incubated with secondary antibody Alexa Flour 488 (Invitrogen) for 2 h, and washed with PBS twice. Hoechst (BD Biosciences, San Jose, CA) was added at 2 μg/ml final concentration and incubated for 15 min. The coverslips are washed with PBS twice and mounted. The imaging was performed using a Leica SP2 DMIRE2 confocal microscope with HCX PL APO lbd.BL 63× 1.4 oil objective.

RESULTS

Kmal Is Affected by SIRT5 and MCD—Our previous studies showed that SIRT5 can catalyze removal of malonyl groups from malonylated lysine residues both *in vitro* and *in vivo* (15). In addition, exogenous malonate can boost lysine malonylation, possibly by increasing intracellular concentrations of malonyl-CoA catalyzed by a short-chain acyl-CoA synthase (15). Consistent with this result, *Sirt5* KO mice showed increased Kmal and Ksucc levels compared with their wild-type counterparts, but not Kac (Fig. 2*A*).

We previously showed, by Western blotting analysis, that Kmal levels are higher in MCD−/− cells than MCD+/+ cells (24). This result, in combination with our earlier observation that malonate can enhance Kmal (15), supports a hypothesis that MCD−/− induces an increase of malonyl-CoA concentration that in turn boosts Kmal. If this is true, a reduction of lipid biosynthesis by reduced activity of fatty-acid synthase may also increase malonyl-CoA and Kmal levels. To test this, we treated both control MCD+/+ and MCD−/− cells with orlistat, an inhibitor of fatty-acid synthase (38). Consistent with our hypothesis, we observed an increase of Kmal levels in response to orlistat in MCD+/+ cells (Fig. 2*B*). In addition, orlistat further increased Kmal levels in MCD−/− cells compared with MCD+/+ cells, whereas Kac and Ksucc levels remained largely unchanged (Fig. 2*C*).

To test whether the enhanced Kmal levels are correlated with higher amounts of malonyl-CoA, we measured intracellular malonyl-CoA levels in MCD+/+ and MCD−/− cells using an HPLC-MS-based metabolomics method. Our data showed that orlistat significantly increased intracellular malonyl-CoA levels in both cell lines (Fig. 2*D*), suggesting that increased lysine malonylation induced via orlistat treatment might be due to enhanced concentration of malonyl-CoA.

Taken together, three different strategies for enhancing malonyl-CoA levels lead to increased levels of lysine malonylation. This result is consistent with our previous work showing that increasing crotonyl-CoA, succinyl-CoA, and glutaryl-CoA levels all result in increases of their respective lysine acylations (11, 13, 39).

Proteomic Identification of Kmal Peptides—Identification of protein substrates is critical to studying the biology of a PTM pathway as was demonstrated in characterization of the lysine acetylation pathway (40–43). To identify Kmal substrate proteins and their modification sites, we used a proteomics approach involving affinity enrichment and subsequent HPLC-MS/MS analysis (Fig. 3). Two experimental models were used: *Sirt5* KO mice and MCD-deficient fibroblasts from malonic aciduria patients. Analysis of Kmal substrates in

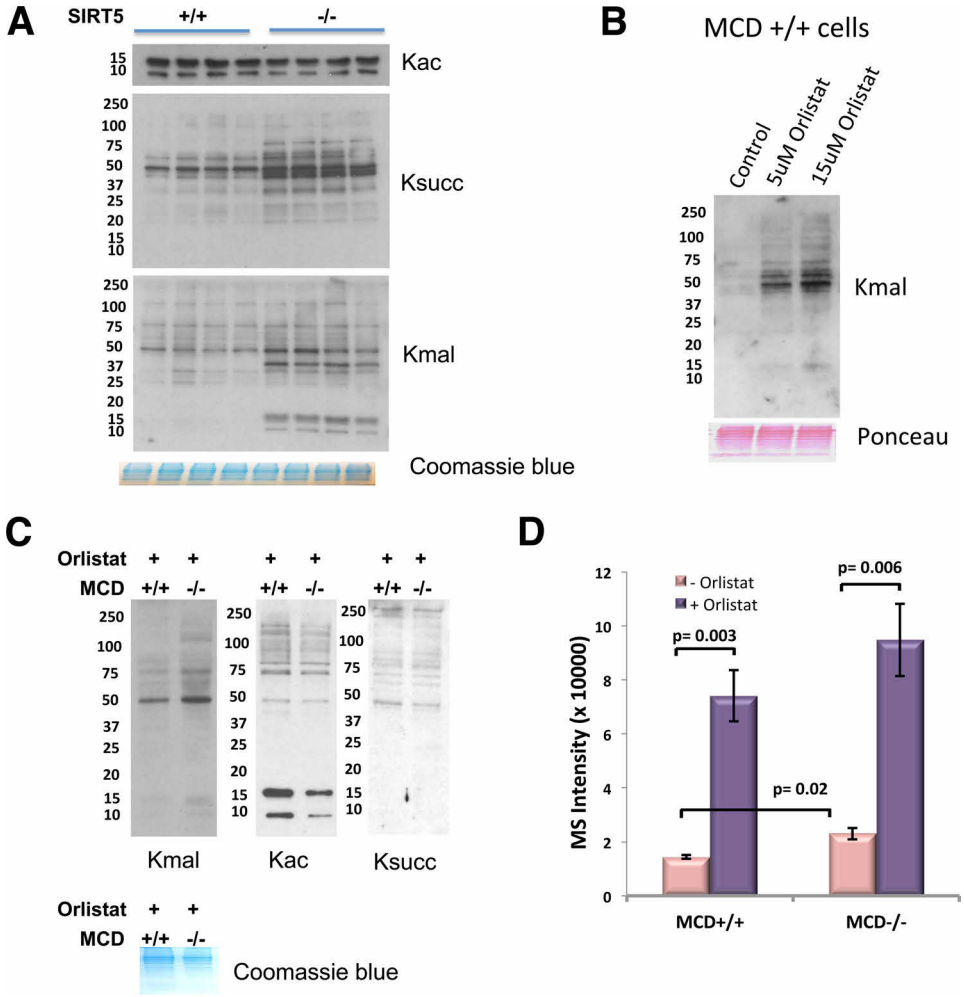

FIG. 2. **Dynamic changes of lysine malonylation *versus* other lysine acylations.** *A*, lysine acylation levels in hepatocytes from (*Sirt5*+/+) and *Sirt5* knock-out (*Sirt5*−/−) mice. Four pairs of mice were used. From *top* to *bottom*, anti-acetyllysine blot, anti-succinyllysine blot, anti-malonyllysine blot, and Coomassie Blue loading control. *B*, MCD+/+ cells treated with 5 and 15 μM orlistat for 48 h. *Top*, anti-malonyllysine blot; *bottom*, Ponceau loading control. *C*, dynamics of lysine acylation in response to orlistat, a fatty acid synthase inhibitor. The MCD+/+ and MCD−/− cells were both treated with 15 μM orlistat for 48 h. From *left* to *right*, anti-malonyllysine blot, anti-acetyllysine blot, anti-succinyllysine blot, and Coomassie Blue loading control. *D*, relative malonyl-CoA levels of MCD+/+ and MCD−/− cells with and without 24-h orlistat treatment. Bars represent S.E. See also supplemental Fig. S1.

mouse liver allows us to identify Kmal substrates in an organ important for cellular metabolism (Fig. 3*A*). The liver also has the highest lysine malonylation levels among the mouse tissues that we screened (supplemental Fig. S1). Quantification of Kmal substrates in MCD-deficient cells *versus* wild-type controls can reveal key Kmal substrates whose modification status is changed in response to malonic aciduria and whose increased malonylation may play a pathogenic role in this disorder (Fig. 3*B*).

Protein extracts from liver tissues of *Sirt5* KO mice were prepared, tryptically digested, and resolved into five fractions by high pH reversed phase HPLC. Kmal peptides were enriched using pan-anti-malonyllysine antibody. The enriched Kmal peptides were analyzed by HPLC-MS/MS (Fig. 3*A*). The acquired raw MS data were analyzed by MaxQuant software with a false discovery rate of 0.01 at protein and peptide levels for the identification of Kmal peptides. To ensure high confidence of the identifications, we removed Kmal peptides with Andromeda scores between 40 and 50 and localization probability below 0.75 prior to bioinformatics analysis (supplemental Table S1A). The Andromeda score is used for ranking the confidence of peptide identifications for the MS/MS spectrum by the Andromeda search engine integrated in MaxQuant software. A higher score indicates a more confident peptide identification. This analysis led to identification of 4016 Kmal sites in 1395 proteins in *Sirt5* KO mouse liver (Fig. 3*C*, *top*). A significant portion of the 427 malonylated peptides (9.6% of the total) with Andromeda scores between 40 and 50 may represent true positives, and these proteins were listed as Kmal candidates (supplemental Table S1B). Annotated spectra of lysine malonylated peptides in mouse liver is included n the supplements.

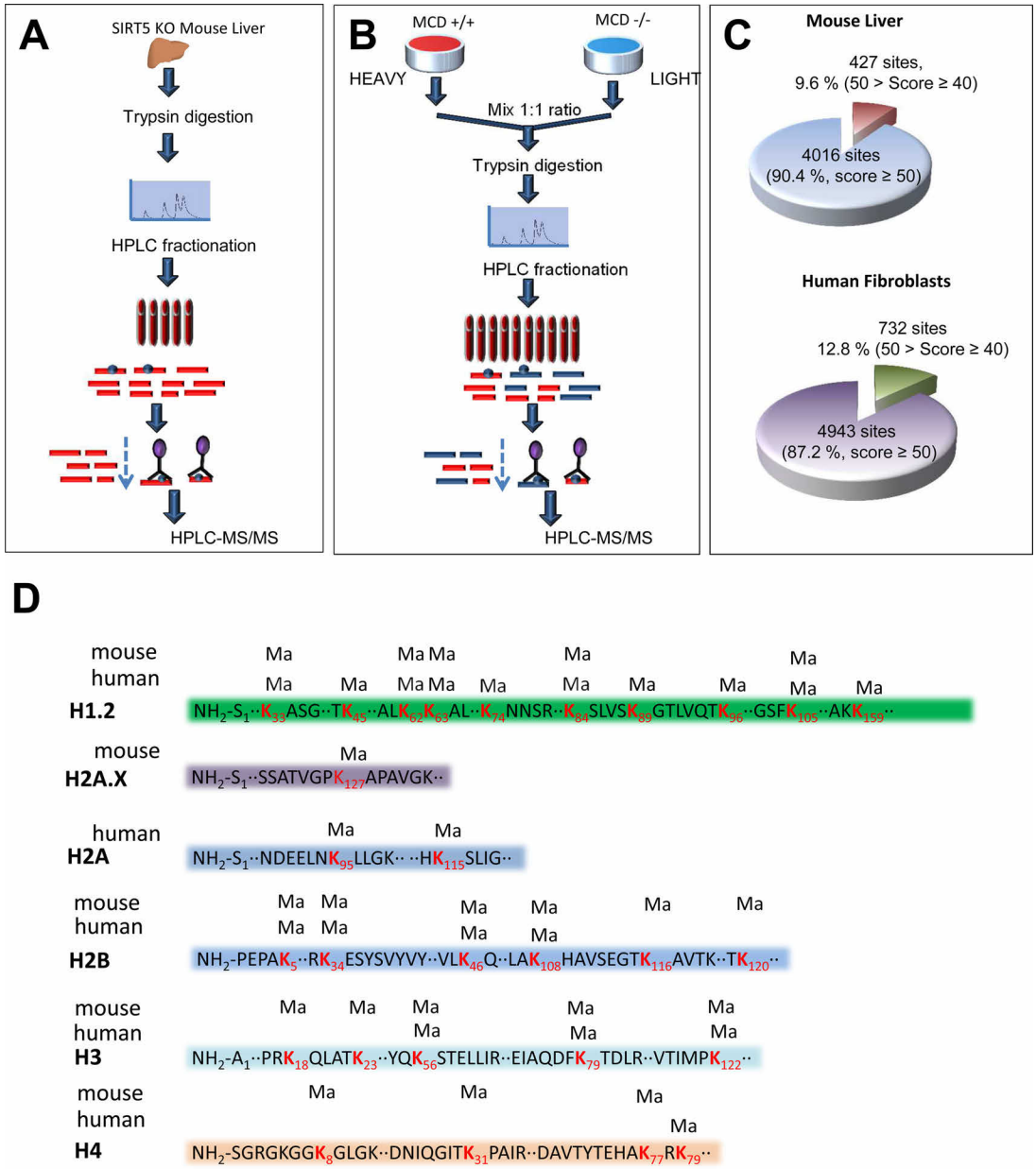

FIG. 3. **Schematic representation of experimental workflow.** *A*, profiling of lysine malonylation substrates in *Sirt5* KO mouse liver. *B*, identification and quantification of lysine malonylation substrates using SILAC and mass spectrometry in MCD+/+ (heavy) and MCD−/− (light) cell lines. *C*, pie charts showing the total numbers of identified lysine malonylated sites in mouse liver (*top*) and MCD+/+ and MCD−/− human cells (*bottom*). The number of Kmal sites with their corresponding MaxQuant Andromeda score ranges and percentiles are indicated. *D*, representation of lysine malonylated (*Ma*) histone sites in mouse and human histones. A_1 and S_1 represent the first alanine and serine residues of the protein, respectively.

In a parallel experiment, we identified and quantified Kmal peptides in human dermal fibroblasts isolated from normal individuals (MCD+/+; labeled with heavy lysine isotope) and from malonic aciduria patients that are deficient in MCD (MCD−/−; labeled with light lysine isotope). Equal amounts of protein lysates from both MCD+/+ and MCD−/− cells were combined in a 1:1 ratio and processed using the same procedure as described above for analysis of Kmal peptides. The study identified 4943 Kmal sites, with Andromeda scores >50, on 1831 proteins in human fibroblasts (MCD+/+ and MCD−/− combined; Fig. 3*C* and supplemental Table S1C). We considered 732 Kmal sites with Andromeda scores between 40 and 50 as the true positive Kmal candidate peptides, and these are listed in supplemental Table S1D. Annotated speactra of lysine malonylated peptides in human cells is included n the supplements.

Among the Kmal substrates, we identified 21 histone marks in mouse liver and 19 histone marks in human fibroblasts

(supplemental Table S2). Interestingly, most of them were not located at N-terminal tails of histones (Fig. 3*D*). Similarly, 35 non-redundant histone lysine succinylation sites have been reported in mouse liver that mostly localize to C-terminal globular domains as well (10). These results suggest that both Kmal and Ksucc histone marks are likely to have a regulatory function different from the widely studied histone acetylation marks (supplemental Table S2).

We previously reported that Ala and Gly were over-represented in the flanking sequences of Ksucc sites, whereas Arg was largely depleted at both −1 and +1 positions (10). Similarly, we evaluated the flanking sequences of Kmal sites to identify whether there was a structural preference for the location of this modification on the peptides. Motif analyses of Kmal sites in mouse liver (supplemental Fig. S2A, left) and human fibroblasts (supplemental Fig. S2B, left) showed significant similarity. Aliphatic amino acids including Ala, Val, Ile, and Gly were over-represented at the flanking sequence of Kmal sites similar to the situation with Ksucc sites, whereas Ser, Pro, and Leu were under-represented. In contrast to the similarity of Kmal and Ksucc flanking sequences, positively charged residues, such as Lys and Arg, predominate in Kac motifs in mouse liver (44).

Quantification of Changes in Kmal Modification Levels from MCD-deficient Cells Versus Wild Type—Using a SILAC-based quantitative proteomics approach, we quantified the difference in Kmal substrate levels between MCD+/+ and MCD−/− cells based on the levels of Kmal peptides and those of protein expression. In parallel, we also quantified changes of protein expression using whole cell lysates derived from a mixture of SILAC labeled MCD+/+ and MCD−/− cells. The changes of Kmal peptides were normalized to the change of their corresponding proteins' levels in MCD cells. Normalized changes of Kmal peptides were used for the subsequent analysis.

Among 4943 Kmal sites on 1822 proteins identified in MCD human fibroblasts, 3181 Kmal sites on 1257 proteins could be quantified (supplemental Table S1, C and D). Among the 1762 unquantified Kmal sites, 1452 are present only in MCD−/− cells (light only); these are the Kmal peptides that have no detected signal in heavy labeled peptide from MCD+/+ cells but significant intensity for the corresponding light labeled peptide from MCD−/− cells by MaxQuant analysis (supplemental Table S1C). The median MCD+/+:MCD−/− ratio of the quantifiable Kmal sites was 0.8284 (Fig. 4*A*). These results clearly suggest that MCD deficiency has an impact on elevating Kmal levels in MCD−/− cells. 461 Kmal sites on 339 proteins increased in abundance by 2-fold or more (normalized $\log_2$ ratio (MCD+/+:MCD−/−) ≤ −1), whereas 1452 Kmal sites on 822 substrate proteins were present in light-only MCD−/− cells (Fig. 4*B* and supplemental Table S1C) Forty-eight Kmal sites on 38 Kmal proteins showed more than a 10-fold increase in MCD−/− cells (supplemental Table S1C). We considered these Kmal substrates to represent the core group of MCD−/− stimulated Kmal substrates. KEGG pathway analysis indicated that these substrates are associated with tricarboxylic acid cycle, oxidative phosphorylation, amino acid degradation (valine, leucine, isoleucine, and lysine), fatty acid metabolism, and propanoate metabolism pathways (supplemental Table S5E).

To calculate the stoichiometry of Kmal in MCD+/+ and MCD−/− cells, we modified a reported algorithm (33) as we described previously (10, 34). The calculation was based on the successful quantification of a Kmal site, its corresponding protein, and the unmodified peptide form in the SILAC experiment (for details, see Ref. 34). To achieve a more accurate calculation, we removed those Kmal sites that were previously reported to be acetylated and succinylated (47, 48) to minimize errors caused by the two modifications at the same residues. This analysis enabled us to calculate the stoichiometry of 325 Kmal sites on 222 proteins in MCD−/− cells with calculated stoichiometries ranging from 0.07 to 50.0% and in MCD+/+ cells with a range from 0.01 to 48.6%, respectively (Fig. 4*C* and supplemental Table S3). The two highest Kmal stoichiometry sites were Lys^{376} of adenylyl cyclase-associated protein 1 (50.0% in MCD−/− cells and 48.6% in MCD+/+ cells) and K41 of phosphoglycerate kinase (49.4% in MCD−/− cells and 48.2% in MCD+/+ cells). VLCAD catalyzes the first step of mitochondrial fatty acid oxidation. Nine Kmal sites were identified in VLCAD among which five sites were detected in MCD−/− cells only, whereas the other four were up-regulated in MCD−/− cells, suggesting a dramatic increase of Kmal on this protein. The dynamic increase of two Kmal sites in VLCAD was 390- and 137-fold, respectively, in MCD−/− cells. Among 324 sites whose stoichiometries were determined, 179 sites (55%) have more than a 2-fold increase of Kmal stoichiometry in MCD−/− cells (supplemental Table S3). For example, malonylation at Lys^{295} of mitochondrial 10-formyltetrahydrofolate dehydrogenase, which is responsible for formate oxidation, is increased from 0.7% in MCD+/+ cells to 31% in MCD−/− cells. Malonylation at Lys^{126} of prohibitin-2, a mediator of transcriptional repression by nuclear hormone receptors, increased from 12.8 to 42.3% in MCD−/− cells.

Overlap among Kmal, Ksucc, and Kac Sites—To understand the similarities and differences among Kmal, Ksucc, and Kac sites, we compared our lysine malonylome data with previously published data (10, 41, 43, 47). We found that, of all the identified Kmal sites in mouse liver, 640 (16%) sites (Fig. 5*A*, *right*) and 595 (42%) proteins (Fig. 5*A*, *left*) overlapped with Kac sites in mouse embryonic fibroblasts (43). Five hundred and ten (36.5%) Kmal sites (Fig. 5*A*, *right*) and 262 (6.5%) proteins (Fig. 5*A*, *left*) overlapped with Ksucc sites in *Sirt5* KO mouse liver (10). When we pooled the Ksucc sites reported in *Sirt5* KO mouse liver and mouse embryonic fibroblasts and carried out the same analysis, 706 (17.6%) sites (supplemental Fig. S2C, right) and 406 (29%) proteins (supplemental Fig. S2C, left) overlapped with Kmal sites identified in *Sirt5* KO

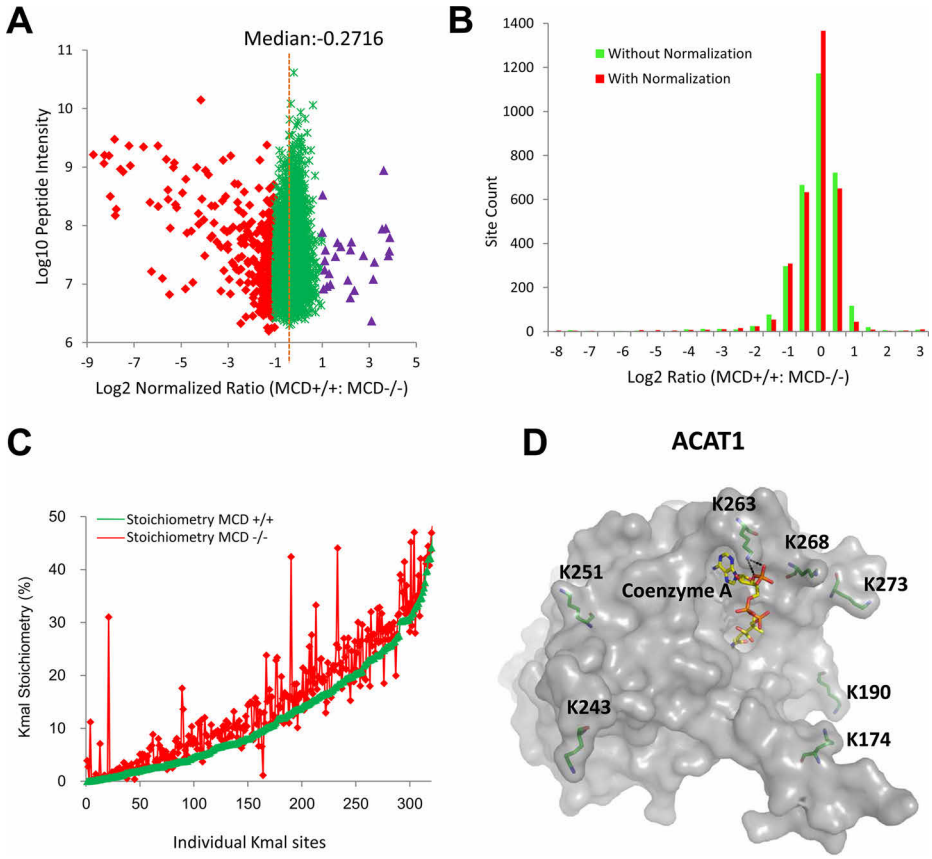

FIG. 4. **Stoichiometry analysis of lysine malonylome.** *A*, scatter plot showing the peptide intensities (*i.e.* the summed precursor ion intensities of each peptide derived from MaxQuant software) of the quantifiable lysine malonylated peptides in relation to their dynamic change in response to MCD knock-out. Kmal ratio (MCD+/+:MCD−/−), MS signal intensity from MCD+/+ divided by that from MCD−/−. *Red*, $\log_2$ ratio (MCD+/+:MCD−/−) ≤ -1; *green*, $-1 \leq \log_2$ ratio (MCD+/+:MCD−/−) ≤ 1; *purple*, $\log_2$ ratio (MCD+/+:MCD−/−) ≥ 1. *B*, histogram showing the distribution of the $\log_2$ ratio (MCD+/+:MCD−/−) SILAC ratios of Kmal sites in MCD+/+ cells over MCD−/− cells. The *y axis* represents the number of Kmal peptides in each category before (*green*) and after (*red*) normalization to the protein amount. *C*, stoichiometry analysis of lysine malonylation sites in MCD+/+ and MCD−/− human fibroblasts. The *x axis* represents individual Kmal sites, and the *y axis* represents the stoichiometry percentage. *D*, three-dimensional protein structure of acetyl-CoA acetyltransferase 1 (ACAT1) shown with lysine malonylation sites (Lys^{190}, Lys^{243}, Lys^{251}, Lys^{263}, Lys^{268}, and Lys^{273}) and the coenzyme A binding site. *Dashed black lines* represent hydrogen bonds.

mouse liver. Interestingly, we found that a significant portion of the malonylated proteins (46.2%) and sites (71.1%) identified in our mouse liver data do not overlap with the previously reported Ksucc and Kac data.

In a parallel experiment, we carried out a similar analysis for the human malonylome. In this experiment, we obtained the Kac and Ksucc data from previous publications (41, 47). Among the Kmal sites identified in human fibroblasts (combination of MCD+/+ and MCD−/−), 776 Kmal sites (Fig. 5*B*, *right*) and Kmal 827 proteins (Fig. 5*B*, *left*) overlapped with the human Kac proteome (41), and 671 sites (Fig. 5*B*, *right*) and 550 proteins (Fig. 5*B*, *left*) overlapped with the human Ksucc proteome (47). Similar to the mouse malonylome data, a significant portion of the human malonylated proteins (46.7%) and sites (75.7%) did not overlap with previously reported Ksucc and Kac data. Overall, the spectrum of lysine sites and protein targets subject to malonylation shows substantial non-overlap with Kac and Ksucc, suggesting that this modification likely plays roles in modulating biological processes distinct from other lysine PTMs.

Cellular Localization of Lysine Malonylomes—SIRT5, a regulatory enzyme of Ksucc, Kglu, and Kmal, localizes predominantly to mitochondria but is also present in the cytosol and nucleus (10, 49). Previously, we reported that 17.8% of Ksucc substrates (351) are localized in the mitochondria in mouse liver (supplemental Fig. S2F, left) (10). Among the Ksucc substrates identified in human cervical cancer cells (HeLa) (47), 17% of Ksucc substrates exclusively localize to mitochondria (supplemental Fig. S2F, right).

To understand the cellular localization of Kmal substrates in mouse liver, we performed the same analysis for the Kmal data set generated from mouse liver. Here, we compared our Kmal data set with the mitochondrial genes annotated in the GO database (50). Of all the identified Kmal substrates, 316 (58%) of them are present in the mitochondria, and 274 (50%) of them are exclusively mitochondrial proteins (Fig. 5*C*, *left*).

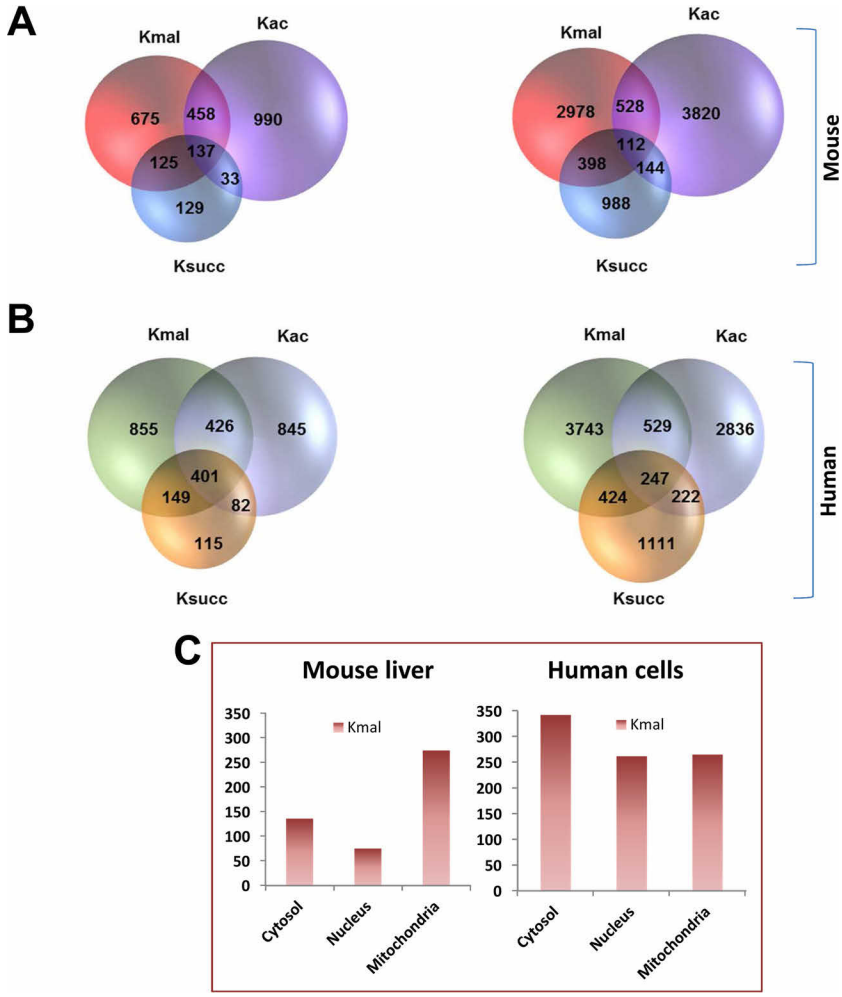

FIG. 5. **Analysis of Kmal substrates *versus* Kac and Ksucc substrates.** *A*, Venn diagrams showing the numbers of overlapping and non-overlapping Kmal, Ksucc, and Kac proteins (*left*) and modification sites (*right*) in the mouse proteome. The mouse Kac and Ksucc data sets were obtained from two previous publications (10, 43). *B*, Venn diagrams showing the numbers of overlapping and non-overlapping Kmal, Ksucc, and Kac proteins (*left*) and modification sites (*right*) in the human proteome. All identified Kmal sites in MCD+/+ and MCD−/− cells were combined for this comparison. The human Kac and Ksucc data sets were from two previous works (41, 47). *C*, graphical representation of subcellular localization of lysine malonylated proteins. In each panel, bar diagrams show the numbers of modified proteins that are exclusively located in the cytosol, nuclei, and mitochondria in mouse liver (*left*) and human cells (*right*). See also supplemental Figs. S2, S6, and Table S7.

Therefore, a comparable fraction of Kmal and Ksucc proteins from mouse liver localizes to mitochondria.

In parallel, we carried out a similar analysis for Kmal proteins derived from human fibroblasts. Our result shows a striking difference of subcellular localization among Kmal substrates. Among the 1024 Kmal substrates identified in human fibroblasts, 338 (33%) of them localize to mitochondria of which 265 (26%) of them are exclusively mitochondrial (Fig. 5*C*, *right*). The number of mitochondrial Kmal substrates from either mouse liver or human fibroblasts is comparable. However, in human fibroblasts, we identified a significantly higher number of nuclear and cytosolic substrates with 262 (30%) and 342 (39%) proteins, respectively (Fig. 5*C*, *right*). The cellular enzymes that catalyze lysine malonylation in mammalian cells are still unknown.

Additionally, we compared the Kmal proteins and sites in mitochondria with our previously reported Ksucc data (10). We found that 198 mitochondrial Kmal proteins (13.9% of all Kmal proteins) (supplemental Fig. S2D, left) and 432 mitochondrial Kmal sites (10.7% all Kmal sites) (supplemental Fig. S2D, right) overlapped with mitochondrial Ksucc in mouse liver, whereas 37% of mitochondrial Kmal proteins and 62% of Kmal sites did not overlap. In human fibroblasts, 59% of mitochondrial Kmal proteins (199) (supplemental Fig. S2E, left) and 31% of mitochondrial Kmal sites (344) (supplemental Fig. S2E, right) overlapped with mitochondrial Ksucc data (47).

We also performed immunostaining of MCD+/+ and MCD−/− human fibroblasts with anti-malonyllysine, anti-acetyllysine, and anti-succinyllysine antibodies along with Hoechst nuclear stain and MitoTracker Red (Fig. 6, *A* and *B*). Our staining results suggest that the strongest signals for Kac and Ksucc are confined in the nucleus in both MCD+/+ and MCD−/− human fibroblasts (Fig. 6, *A* and *B*, *second* and *third rows*). However, Kmal signals are distributed among the cytosol and nucleus in MCD+/+ cells (Fig. 6*A*, *top row*). Interestingly, most of the Kmal signal overlaps with MitoTracker Red in MCD−/− cells (Fig. 6*B*, *top row*), suggesting that Kmal levels increase specifically in the mitochondria of MCD−/− cells.

Functional Annotation of Lysine Malonylomes—To understand the biological functions of Kmal proteins, we performed enrichment analysis by using the GO database (30) and KEGG (51) for Kmal substrates identified in mouse liver and human

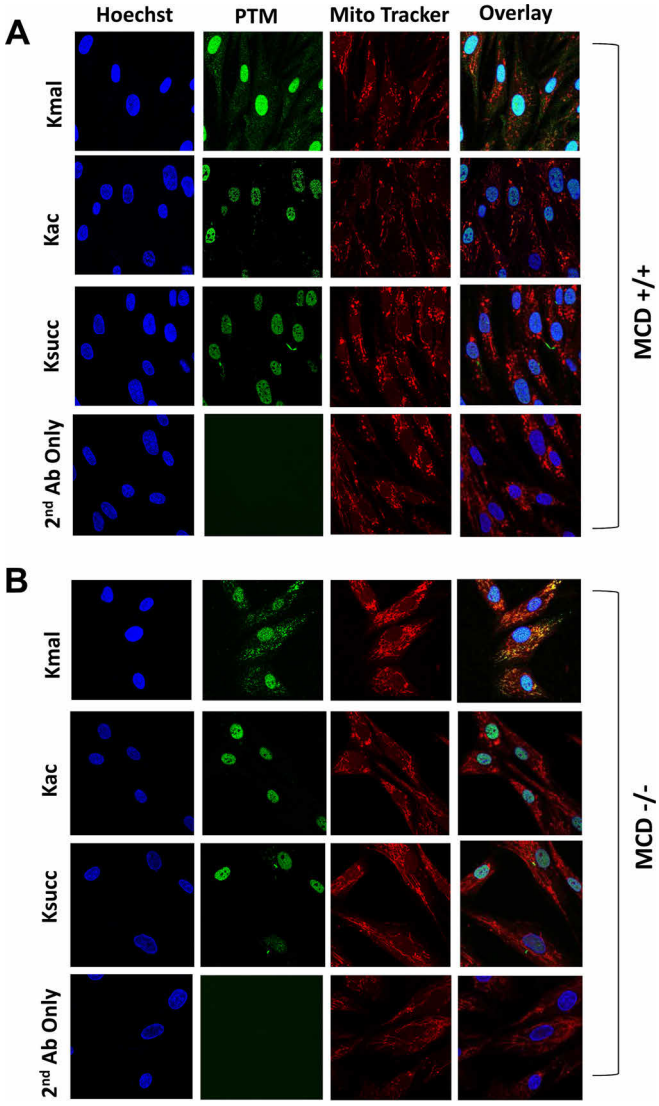

FIG. 6. **Immunocytochemistry imaging of MCD+/+ (*A*) and MCD−/− (*B*) cells.** *Top* to *bottom*, Kmal, Kac, and Ksucc staining, and second antibody (*Ab*) only (negative) control. *Left* to *right*, Hoechst nuclear stain, corresponding PTM, MitoTracker Red (*Mito*), and overlapped channels.

fibroblasts. The GO biological process analysis of mouse liver Kmal substrates (supplemental Table S4) showed enrichment in oxidation/reduction (adj $p = 5.45 \times 10^{-51}$), protein translation (adj $p = 5.71 \times 10^{-49}$), cofactor metabolism (adj $p = 4.18 \times 10^{-26}$), and fatty acid metabolism (adj $p = 5.09 \times 10^{-12}$) (supplemental Fig. S3A, left). The GO analysis of human fibroblast malonylome (supplemental Fig. S3B, left and supplemental Table S5) showed enrichment in protein expression processes, such as translation (adj $p = 2.22 \times 10^{-55}$), translation elongation (adj $p = 7.43 \times 10^{-26}$), tRNA aminoacylation (adj $p = 1.01 \times 10^{-20}$), and intracellular transport (adj $p = 5.30 \times 10^{-31}$). Proteins associated with fatty acid β-oxidation were also enriched in the human fibroblast malonylome (adj $p = 2.34 \times 10^{-7}$; supplemental Table S5).

The molecular function analysis of mouse liver Kmal substrates showed enrichment in nucleotide binding (adj $p = 9.35 \times 10^{-35}$), cofactor binding (adj $p = 1.04 \times 10^{-27}$), and ATP binding (adj $p = 1.86 \times 10^{-15}$) (supplemental Fig. S3A, right). Kmal substrates in human fibroblasts were associated with nucleotide binding (adj $p = 3.22 \times 10^{-45}$), nucleoside binding (adj $p = 2.77 \times 10^{-29}$), ATP binding (adj $p = 4.73 \times 10^{-26}$), and aminoacyl-tRNA ligase activity (adj $p = 2.74 \times 10^{-20}$) (supplemental Fig. S3B, right), supporting the idea that Kmal may be involved in regulating protein translation.

There was no significant difference between GO (supplemental Fig. S4A) and KEGG pathway enrichments (supplemental Fig. S4B) of all the proteins identified in human fibroblasts *versus* light-only protein substrates derived from MCD−/− cells (supplemental Table S6). In addition, there was a significant overlap between the KEGG pathway analysis of mouse liver (supplemental Fig. S3C) and that of human fibroblasts (supplemental Fig. S3D). The top enriched categories of KEGG pathways for lysine-malonylated substrates were ribosome, valine/leucine/isoleucine degradation, proteasome, and fatty acid metabolism (supplemental Fig. S3, C and D). Twenty-nine of 45 key enzymes in mouse and 22 of 45 key enzymes in humans involved in regulation of fatty acid metabolism were lysine malonylated (supplemental Fig. S5, A and B and supplemental Table S5F). Among these, five enzymes (fatty-acid synthase, acetyl-CoA carboxylase 1, ATP-citrate lyase, AMP-activated protein kinase, and CPT1) are closely associated with malonyl-CoA metabolism (supplemental Fig. S5C).

Of particular note are a few proteins involved in fatty acid metabolism. We found that acetyl-CoA acetyltransferase 1, an enzyme participating in multiple metabolic pathways including fatty acid metabolism, was malonylated at seven sites: Lys^{174}, Lys^{190}, Lys^{243}, Lys^{251}, Lys^{263}, Lys^{268}, and Lys^{273} (Fig. 4*D*). The Kmal level of (MCD+/+: MCD−/− SILAC ratio of 0.0044) Lys^{263} of acetyl-CoA acetyltransferase 1 was increased more than 200-fold in MCD−/− cells. Lys^{263} is in close proximity with the coenzyme A binding site and possibly makes two hydrogen bonds with coenzyme A, suggesting a possibility that this residue is important in regulating the protein's function. Lys^{263} was previously reported to be acetylated and succinylated as well (41, 47). In addition, among all the Kmal sites of acetyl-CoA acetyltransferase 1, Lys^{174} is acetylated, and Lys^{251} is succinylated (41). Therefore, these Kmal sites might also contribute to regulation of protein function depending on the type of modification. Hydroxymethylglutaryl-CoA lyase is malonylated at three lysine sites (Lys^{48}, Lys^{93}, and Lys^{137}) of which Lys^{48} malonylation is increased roughly 39-fold in MCD−/− cells. Hydroxymethylglutaryl-CoA lyase exclusively localizes to mitochondria and is specifically responsible for leucine degradation as well as ketone production during fat breakdown. Hydroxymethylglutaryl-CoA lyase deficiency is a rare genetic disease that causes metabolic acidosis and hypoglycemia (52). A K-to-N mutation at Lys^{48}

of hydroxymethylglutaryl-CoA lyase ablates enzymatic activity, which suggests that K48 is a critical position for enzymatic function (53). Therefore, lysine malonylation of Lys^{48} may lead to changes in enzymatic activity of this protein. ATP-citrate lyase catalyzes conversion of citrate to acetyl-CoA (supplemental Fig. S5C), which can be converted further to malonyl-CoA by acetyl-CoA carboxylase 1. Among the 14 Kmal sites in ATP-citrate lyase, Lys^{68}, which is located next to an ATP binding site (Lys^{66}-Lys^{67}), is malonylated and therefore might alter the ATP binding ability of the protein. Enrichment of fatty acid metabolism proteins in the malonylomes in both mouse liver and human fibroblasts suggests a possible feedback regulation of fatty acid biosynthesis by malonyl-CoA-mediated lysine malonylation.

Mitochondrial Function and Fatty Acid Oxidation Are Impaired in MCD−/− Cells—Integration of our bioinformatics analyses of lysine malonylated proteins identified in mouse liver and human fibroblasts demonstrates that among metabolic pathways proteins involved in fatty acid metabolism were preferentially heavily malonylated. Fatty acid synthesis, which utilizes malonyl-CoA as a substrate for synthesis and chain elongation, primarily occurs in the cytosol, whereas fatty acid oxidation occurs in mitochondria and peroxisomes. Because MCD−/− cells showed greatly increased Kmal immunostaining in mitochondria compared with MCD+/+ cells (Fig. 6) and MCD-deficient patients have been reported to present with pathologies similar to those of patients with fatty acid oxidation defects, we wanted to understand whether mitochondrial function and fatty acid oxidation are affected in MCD−/− cells. Long-chain fatty acids are broken down to medium- and short-chain fatty acids in mitochondria by VLCAD and medium-chain acyl-CoA dehydrogenase together with the mitochondrial trifunctional protein complex encoded by the *Hadha* and *Hadhb* genes. Mitochondrial trifunctional protein complex consists of LCHAD, long-chain enoyl-CoA hydratase, and long-chain keto-acyl-CoA thiolase enzymatic activities. In MCD−/− cells, multiple mitochondrial fatty acid oxidation proteins were heavily malonylated, and both VLCAD and trifunctional enzyme subunit alpha were substantially more malonylated than in wild-type cells (Fig. 7*A* and supplemental Fig. S7B). Many of the detectable malonylated lysine sites were only present in MCD−/− cells. Examination of the crystal structure of VLCAD (Protein Data Bank codes 2UXW and 3B96) reveals that sites of lysine malonylation are scattered across the polypeptide (Fig. 7*B*). Three of the Kmal sites (Lys^{278}, Lys^{331}, and Lys^{480}) occupy highly conserved amino acid positions among VLCAD orthologues. A majority of the lysine sites are surface-exposed, and their malonylation may impact different properties of the protein: three (Lys^{480}, Lys^{482}, and Lys^{55}) are located at the putative surface of membrane attachment (54), two (Lys^{635} and Lys^{639}) are found in proximity to the dimerization interface, and three (K^{276}, K^{278}, and K^{331}) are positioned near the active site where FAD and acyl-CoA molecules bind (Fig. 7*B*). We next analyzed whether VLCAD enzymatic activity was affected by malonylation in MCD−/− cells. Indeed, VLCAD activity was decreased 45% in MCD−/− cells as compared with MCD+/+ cells (Fig. 7*C*). Basal expression levels of VLCAD protein were similar in MCD+/+ and MCD−/− cells (supplemental Fig. S7A). Furthermore, the LCHAD activity of mitochondrial trifunctional protein was significantly decreased in MCD−/− cells as well (Fig. 7*D*).

Accumulation of cytosolic malonyl-CoA is known to inhibit CPT1, which is located on the outer membrane of the mitochondria. CPT1, together with carnitine-acylcarnitine translocase and CPT2, imports acyl-CoAs into the mitochondria for β-oxidation. Our data now suggest that an increase of lysine malonylation on proteins within the mitochondrial matrix can also inhibit fatty acid oxidation. To test whether mitochondrial function and fatty acid oxidation are indeed affected by lysine malonylation, we studied the impact of malonate on mitochondrial function in Fao liver cells. Previously, we have shown that malonate treatment induces significant lysine malonylation (15). To eliminate any confounding effects from direct interference of malonate itself on mitochondrial function, we treated cells with malonate for 1 day followed by a malonate-free overnight incubation prior to analysis of mitochondrial function. Malonate treatment of cells significantly reduced the OCR in the context of pyruvate, succinate, and octanoylcarnitine mitochondrial oxidation (Fig. 7, *E*, *F*, and *G*). CPT1 is not required for oxidation of octanoylcarnitine; hence, inhibition of CPT1 by malonyl-CoA cannot explain the observed decrease in OCR in the presence of octanoylcarnitine. Instead, this finding likely indicates that either oxidative phosphorylation or fatty acid oxidation activity is decreased by lysine malonylation.

Finally, we analyzed both succinate- and octanoylcarnitine-driven OCR in MCD−/− and MCD+/+ cells. Interestingly, succinate-driven OCR was only mildly reduced in MCD−/− cells (Fig. 7, *H* and *J*), whereas octanoylcarnitine-driven OCR was 40% decreased in MCD−/− cells as compared with MCD+/+ cells (Fig. 7, *I* and *J*). Together, these findings suggest that malonyl-CoA can inhibit mitochondrial fatty acid oxidation in MCD−/− cells, possibly through elevated lysine malonylation, independently of effects on CPT1.

DISCUSSION

In this study, we performed the first global proteomic analysis of the lysine malonylome by using *Sirt5* KO mouse liver and human dermal fibroblasts. Overall, we identified 4042 lysine malonylated peptides in 1426 proteins in *Sirt5* KO mouse liver and 4943 malonylated peptides in 1822 proteins in human fibroblasts. Four hundred sixty-one Kmal sites on 339 proteins showed a 2-fold increase or more in MCD−/− cells relative to MCD+/+ cells, and 1452 Kmal sites on 822 proteins were only detected in MCD−/− cells, suggesting that MCD activity has a profound impact on Kmal levels.

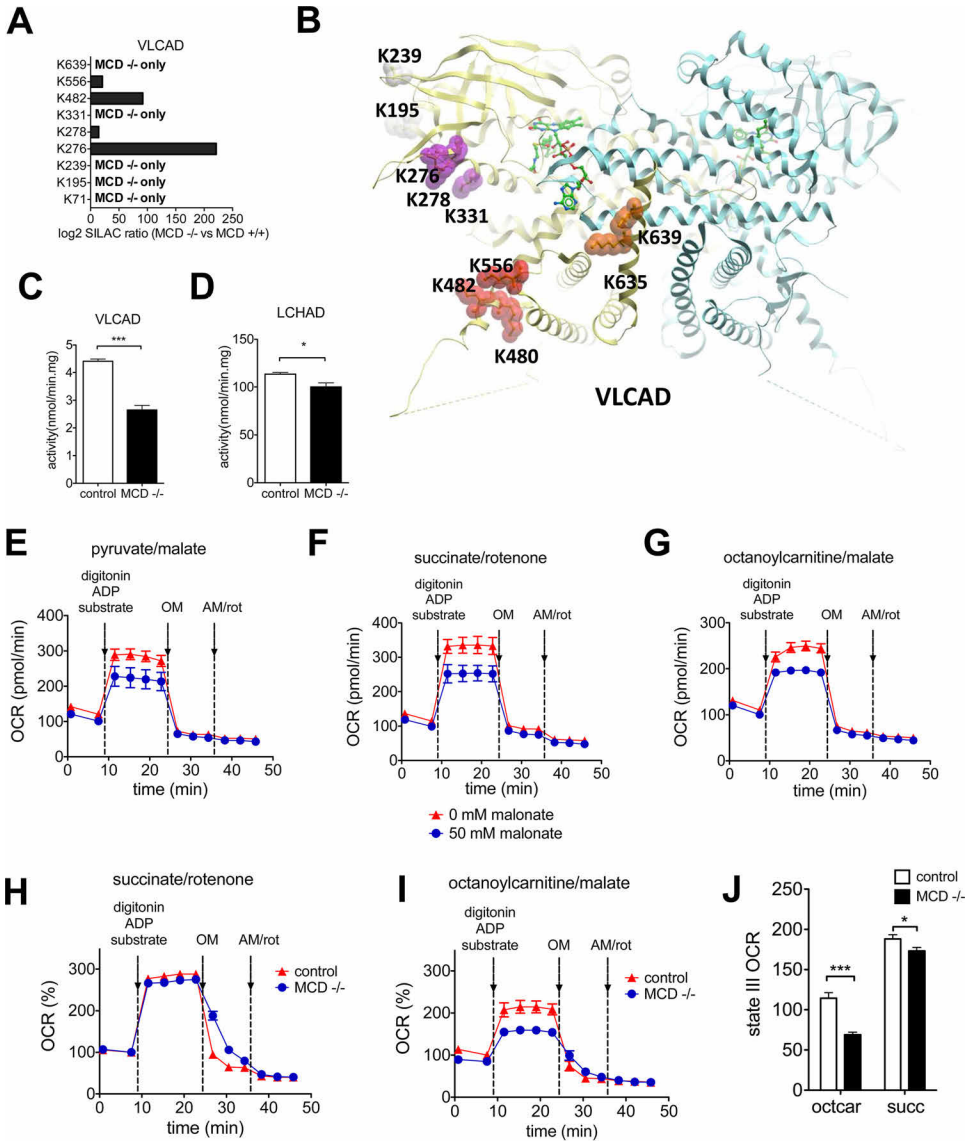

FIG. 7. **Lysine malonylation impacts mitochondrial function and fatty acid oxidation.** *A*, the SILAC ratios of lysine malonylation sites of VLCAD determined by quantitative proteomics between MCD+/+ and MCD−/− fibroblast cells, respectively. A number of malonylated lysines were only detected in MCD−/− cells. *B*, VLCAD protein structure with mapped lysine malonylation sites (Protein Data Bank codes 2UXW and 3B96). *C*, palmitoyl-CoA dehydrogenase activity of the VLCAD enzyme in cell lysates from MCD+/+ and MCD−/− cells. *Bars* represent means ± S.E. (n = 3–6). *D*, 3-keto-palmitoyl-CoA dehydrogenase activity of the LCHAD enzyme in cell lysates from MCD+/+ and MCD−/− cells. *Bars* represent means ± S.E. (n = 3). *E–G*, respiration analysis of digitonin-permeabilized Fao hepatoma cells that were exposed to 50 mM malonate for 1 day followed by overnight incubation in malonate-free medium (see text for details). Respiration analysis was performed with pyruvate/malate (*E*), succinate/rotenone (*F*), or octanoylcarnitine/malate (*G*). *H–J*, respiration analysis of digitonin-permeabilized MCD+/+ and MCD−/− fibroblasts similar to *F* and *G*. *OM*, oligomycin; *AM/rot*, antimycin/rotenone; *octcar*, octanoylcarnitine; *succ*, succinate. *, p value <0.05; ***, p value <0.001. Bars represent mean +/− S.E. See also supplemental Fig. S7.

Our analysis revealed intriguing differences between Kmal substrates *versus* other lysine PTMs (10, 41). First, Kmal substrates show divergent cellular localization patterns between liver and fibroblast cells (Fig. 5*C*). In mouse liver, Kmal and Ksucc predominantly localized to mitochondria with a small number of substrate proteins in the cytosol and nucleus. In contrast, in the case of MCD+/+ human fibroblasts, Kmal proteins were distributed among the cytosol and nucleus (Fig. 5*C*, *right*), whereas in MCD−/− cells, increased localization of Kmal substrates in the mitochondria was observed. Malonyl-CoA is reported to localize to extracellular, membrane, mitochondrial, and peroxisomal spaces of the cell according to the Human Metabolome Database. The concentration of malonyl-CoA in mitochondria is not known. It is likely that mitochondrial malonyl-CoA is the cofactor for the lysine malonylation reaction.

Second, the identification of a large number of Kmal substrates in the cytosol and nucleus of human fibroblasts sug-

gests the potential existence of an enzyme(s) catalyzing transfer of malonyl groups from malonyl-CoA to lysine residues. It has been proposed that this process occurs non-enzymatically in the high pH chemical environment of mitochondria (4, 47, 55). However, this *in vitro* spontaneous protein acylation cannot exclude the possibility of an enzyme-catalyzed PTM reaction as in the case of lysine acetylation, which can occur via both non-enzymatic and enzyme-catalyzed reactions. Given the fact that the pH is lower in the cytosol and nucleus than in mitochondria and that the subcellular localization of Kmal substrates is very different in liver *versus* fibroblasts, it is possible that there is significant enzyme-catalyzed lysine malonylation outside mitochondria in human fibroblasts.

Third, as many as 2693 Kmal sites remain at similar levels (with less than a 2-fold change) in human fibroblasts with or without the expression of MCD enzyme. Cellular localization analysis showed that these Kmal substrates were not enriched in mitochondria. In stark contrast, the proteins showing increased Kmal in MCD deficiency (more than 2-fold change) were enriched in the mitochondrion (supplemental Table S6F). This suggests that the increased Kmal occurring in the context of MCD deficiency primarily impacts mitochondrial functions including respiration. Indeed, we showed that lysine malonylation inhibited mitochondrial function and impaired octanoylcarnitine oxidation in MCD−/− cells. Because mitochondrial octanoylcarnitine oxidation does not require CPT1, our studies demonstrate that malonyl-CoA can also impact fatty acid oxidation and mitochondrial function via malonylation of proteins located in the mitochondrial matrix independently of CPT1. This implies that malonyl-CoA can play a major role in controlling mitochondrial function by lysine malonylation of mitochondrial matrix proteins.

Diverse pathological symptoms have been observed in patients with inborn MCD deficiency, several of which are also common in fatty acid oxidation disorders, such as cardiomyopathy, muscle weakness, and hypoglycemia (56, 57). This observation has led to the hypothesis that CPT1 inhibition by elevated malonyl-CoA levels could play a role in the pathophysiology of MCD deficiency. Indeed, palmitate and myristate oxidation was severely reduced in MCD-deficient patient fibroblasts, implying a possible role of malonyl-CoA in inhibition of fatty acid oxidation in the pathogenesis of this disorder (58). In light of our result that malonyl-CoA accumulation can impact metabolic pathways via CPT1-independent lysine malonylation, it seems likely that accumulation of mitochondrial lysine malonylation also plays a pathogenic role in MCD deficiency. Moreover, KEGG pathway analysis of Kmal substrates showed enrichment of the modification in pathways besides those associated with fatty acid metabolism. MCD-deficient patients can suffer from delayed neurological development (59). Although the pathogenic mechanism of this effect is still not well understood, it has been suggested that disruption of the interaction between malonyl-CoA and CPT1 might be a cause (45). Our data suggest that elevated Kmal on many mitochondrial proteins may represent another mechanism of the pathology associated with malonic aciduria. Because Kmal levels are regulated by SIRT5, this raises the possibility that pharmacologic strategies to increase SIRT5 activity may represent a rational treatment strategy in MCD deficiency.

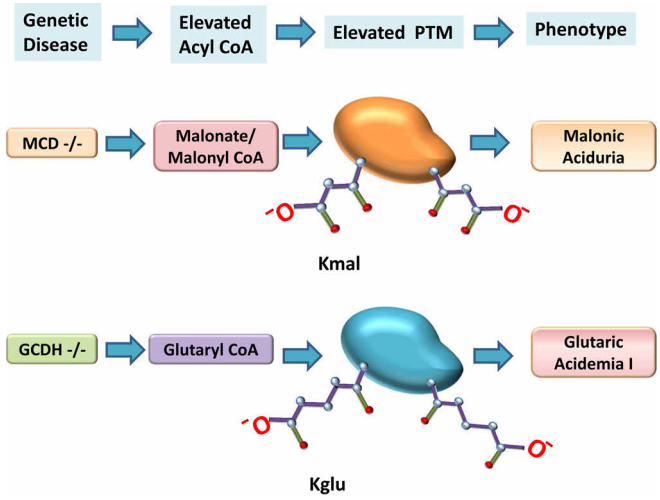

FIG. 8. **Graphical abstract: schematic illustration of hypothetical mechanisms of how Kmal and Kglu may contribute to disease phenotype.** MCD and glutaryl-CoA dehydrogenase (*GCDH*) deficiencies lead to elevated malonate/malonyl-CoA (*top*) and glutarate/glutaryl CoA (*bottom*) levels, respectively. This can cause dynamic changes in Kmal (*top*) and Kglu (*bottom*), which may contribute to disease phenotypes of patients with MCD deficiency and glutaryl-CoA dehydrogenase deficiency.

Identification, characterization, and proteomic screening of three acidic lysine acylation pathways, malonylation, succinylation, and glutarylation, suggest association of these pathways with multiple inborn metabolic diseases. In this study, our results suggest that elevated malonic acid in MCD-deficient cells can induce an increase of Kmal levels in substrate proteins that in turn might impair the activities of key cellular metabolic enzymes, such as VLCAD and LCHAD. Glutaric acidemia I (OMIM 231670) is caused by homozygous or compound heterozygous mutations in the gene encoding glutaryl-CoA dehydrogenase. A previous study demonstrated that glutaric acidemia I patients as well as glutaryl-CoA dehydrogenase KO mice display increased levels of glutaryl-CoA (14). We showed that glutarylation suppresses carbamoyl-phosphate synthase 1 enzymatic activity in cell lines, mice, and a model of glutaric acidemia type I disease. This result suggests that up-regulation of glutaric acid and glutaryl-CoA can lead to elevated levels of Kglu that in turn modulate activities of at least some substrate proteins (11). Additionally, we previously demonstrated that lysine propionylation and lysine butyrylation also accumulate in propionyl-CoA carboxylase deficiency and short-chain acyl-CoA dehydrogenase deficiency, respectively (24). Furthermore, mutations in the genes that are involved in succinyl-CoA metabolism, such as ketoglutarate

dehydrogenase, succinyl-CoA-3-ketoacid-coenzyme A transferase, and succinyl-CoA ligase, lead to metabolic diseases (46). Weinert *et al.* (47) demonstrated that loss of succinyl-CoA ligase in yeast results in increased lysine succinylation, suggesting that accumulation of mitochondrial succinyl-CoA can increase mitochondrial succinylation. Taken together, a new hypothesis has emerged from studies of these acidic lysine acylations: elevated levels of acyl-CoA can induce lysine acylation in substrate proteins that may modulate their functions and possibly contribute to disease (Fig. 8).

Mechanistic understanding of Kmal, Ksucc, and Kglu pathway dysregulation in inborn metabolic diseases may be relevant for developing novel therapeutic strategies for these diseases. For example, it may be possible to activate SIRT5 and alleviate the symptomatology in these conditions. Moreover, this mechanistic understanding can be instrumental for the analysis of the role of lysine acylation in other diseases, such as diabetes and cancer, where disturbance of metabolic homeostasis plays a critical role.

Acknowledgment—We thank the Cell Line and DNA Biobank from Patients Affected by Genetic Diseases (Instituto G. Gaslini) (Project GTB12001), funded by Telethon Italy, for providing cell lines.

Addendum—During the course of this submission, a paper describing proteomic analysis of lysine malonylation was published in *Molecular Cell* (60).

* This work was supported, in whole or in part, by National Institutes of Health Grants GM105933 and CA160036 (to Y. Z.), R01GM101171 and R21CA177925 (to D. B. L., T32-AG000114 (to J. P.), and R00CA168997 (to J. W. L.).

S This article contains supplemental Figs. S1–S7, Tables S1–S7, and annotated spectra.

[b] These authors made equal contributions to this work.

[e] Supported by National Science and Technology Major Project of the Ministry of Science and Technology of China Grant 2012ZX09301001-007), National Basic Research Program of China 973 Program Grant 2014CBA02004, Natural Science Foundation of China Grant 31370814, and Shanghai Pujiang Program Grant 13PJ1410300.

[k] Supported by Netherlands Organization for Scientific Research VENI Grant 916.10.065 and the Academic Medical Center, Amsterdam, The Netherlands. To whom correspondence may be addressed. Tel.: 31-20-566-3927; E-mail: v.c.deboer@amc.uva.nl.

[l] To whom correspondence may be addressed. Tel.: 773-834-1561; E-mail: yingming.zhao@uchicago.edu.

REFERENCES

1. Roth, S. Y., Denu, J. M., and Allis, C. D. (2001) Histone acetyltransferases. *Annu. Rev. Biochem.* **70,** 81–120
2. Yang, X. J., and Seto, E. (2007) HATs and HDACs: from structure, function and regulation to novel strategies for therapy and prevention. *Oncogene* **26,** 5310–5318
3. Chang, H. C., and Guarente, L. (2014) SIRT1 and other sirtuins in metabolism. *Trends Endocrinol. Metab.* **25,** 138–145
4. Wagner, G. R., and Hirschey, M. D. (2014) Nonenzymatic protein acylation as a carbon stress regulated by sirtuin deacylases. *Mol. Cell* **54,** 5–16
5. Giblin, W., Skinner, M. E., and Lombard, D. B. (2014) Sirtuins: guardians of mammalian healthspan. *Trends Genet.* **30,** 271–286
6. Haberland, M., Montgomery, R. L., and Olson, E. N. (2009) The many roles of histone deacetylases in development and physiology: implications for disease and therapy. *Nat. Rev. Genet.* **10,** 32–42
7. Lee, J. H., Choy, M. L., and Marks, P. A. (2012) Mechanisms of resistance to histone deacetylase inhibitors. *Adv. Cancer Res.* **116,** 39–86
8. Xie, Z., Dai, J., Dai, L., Tan, M., Cheng, Z., Wu, Y., Boeke, J. D., and Zhao, Y. (2012) Lysine succinylation and lysine malonylation in histones. *Mol. Cell. Proteomics* **11,** 100–107
9. Du, J., Zhou, Y., Su, X., Yu, J. J., Khan, S., Jiang, H., Kim, J., Woo, J., Kim, J. H., Choi, B. H., He, B., Chen, W., Zhang, S., Cerione, R. A., Auwerx, J., Hao, Q., and Lin, H. (2011) Sirt5 is a NAD-dependent protein lysine demalonylase and desuccinylase. *Science* **334,** 806–809
10. Park, J., Chen, Y., Tishkoff, D. X., Peng, C., Tan, M., Dai, L., Xie, Z., Zhang, Y., Zwaans, B. M., Skinner, M. E., Lombard, D. B., and Zhao, Y. (2013) SIRT5-mediated lysine desuccinylation impacts diverse metabolic pathways. *Mol. Cell* **50,** 919–930
11. Tan, M., Peng, C., Anderson, K. A., Chhoy, P., Xie, Z., Dai, L., Park, J., Chen, Y., Huang, H., Zhang, Y., Ro, J., Wagner, G. R., Green, M. F., Madsen, A. S., Schmiesing, J., Peterson, B. S., Xu, G., Ilkayeva, O. R., Muehlbauer, M. J., Braulke, T., Mühlhausen, C., Backos, D. S., Olsen, C. A., McGuire, P. J., Pletcher, S. D., Lombard, D. B., Hirschey, M. D., and Zhao, Y. (2014) Lysine glutarylation is a protein posttranslational modification regulated by SIRT5. *Cell Metab.* **19,** 605–661
12. Dai, L., Peng, C., Montellier, E., Lu, Z., Chen, Y., Ishii, H., Debernardi, A., Buchou, T., Rousseaux, S., Jin, F., Sabari, B. R., Deng, Z., Allis, C. D., Ren, B., Khochbin, S., and Zhao, Y. (2014) Lysine 2-hydroxyisobutyrylation is a widely distributed active histone mark. *Nat. Chem. Biol.* **10,** 365–370
13. Tan, M., Luo, H., Lee, S., Jin, F., Yang, J. S., Montellier, E., Buchou, T., Cheng, Z., Rousseaux, S., Rajagopal, N., Lu, Z., Ye, Z., Zhu, Q., Wysocka, J., Ye, Y., Khochbin, S., Ren, B., and Zhao, Y. (2011) Identification of 67 histone marks and histone lysine crotonylation as a new type of histone modification. *Cell* **146,** 1016–1028
14. Koeller, D. M., Woontner, M., Crnic, L. S., Kleinschmidt-DeMasters, B., Stephens, J., Hunt, E. L., and Goodman, S. I. (2002) Biochemical, pathologic and behavioral analysis of a mouse model of glutaric acidemia type I. *Hum. Mol. Genet.* **11,** 347–357
15. Peng, C., Lu, Z., Xie, Z., Cheng, Z., Chen, Y., Tan, M., Luo, H., Zhang, Y., He, W., Yang, K., Zwaans, B. M., Tishkoff, D., Ho, L., Lombard, D., He, T. C., Dai, J., Verdin, E., Ye, Y., and Zhao, Y. (2011) The first identification of lysine malonylation substrates and its regulatory enzyme. *Mol. Cell. Proteomics* **10,** M111.012658
16. Saggerson, D. (2008) Malonyl-CoA, a key signaling molecule in mammalian cells. *Annu. Rev. Nutr.* **28,** 253–272
17. Wolfgang, M. J., and Lane, M. D. (2008) Hypothalamic malonyl-coenzyme A and the control of energy balance. *Mol. Endocrinol.* **22,** 2012–2020
18. Bandyopadhyay, G. K., Yu, J. G., Ofrecio, J., and Olefsky, J. M. (2006) Increased malonyl-CoA levels in muscle from obese and type 2 diabetic subjects lead to decreased fatty acid oxidation and increased lipogenesis; thiazolidinedione treatment reverses these defects. *Diabetes* **55,** 2277–2285
19. Fillmore, N., and Lopaschuk, G. D. (2014) Malonyl CoA: a promising target for the treatment of cardiac disease. *IUBMB Life* **66,** 139–146
20. Abu-Elheiga, L., Oh, W., Kordari, P., and Wakil, S. J. (2003) Acetyl-CoA carboxylase 2 mutant mice are protected against obesity and diabetes induced by high-fat/high-carbohydrate diets. *Proc. Natl. Acad. Sci. U.S.A.* **100,** 10207–10212
21. Tong, L., and Harwood, H. J., Jr. (2006) Acetyl-coenzyme A carboxylases: versatile targets for drug discovery. *J. Cell. Biochem.* **99,** 1476–1488
22. FitzPatrick, D. R., Hill, A., Tolmie, J. L., Thorburn, D. R., and Christodoulou, J. (1999) The molecular basis of malonyl-CoA decarboxylase deficiency. *Am. J. Hum. Genet.* **65,** 318–326
23. Santer, R., Fingerhut, R., Lässker, U., Wightman, P. J., Fitzpatrick, D. R., Olgemöller, B., and Roscher, A. A. (2003) Tandem mass spectrometric determination of malonylcarnitine: diagnosis and neonatal screening of malonyl-CoA decarboxylase deficiency. *Clin. Chem.* **49,** 660–662
24. Pougovkina, O., Te Brinke, H., Wanders, R. J., Houten, S. M., and de Boer, V. C. (2014) Aberrant protein acylation is a common observation in inborn errors of acyl-CoA metabolism. *J. Inher. Metab. Dis.* **37,** 709–714
25. Lombard, D. B., Alt, F. W., Cheng, H. L., Bunkenborg, J., Streeper, R. S., Mostoslavsky, R., Kim, J., Yancopoulos, G., Valenzuela, D., Murphy, A., Yang, Y., Chen, Y., Hirschey, M. D., Bronson, R. T., Haigis, M., Guarente, L. P., Farese, R. V., Jr., Weissman, S., Verdin, E., and Schwer, B. (2007)

Mammalian Sir2 homolog SIRT3 regulates global mitochondrial lysine acetylation. *Mol. Cell. Biol.* **27,** 8807–8814
26. Nakagawa, T., Lomb, D. J., Haigis, M. C., and Guarente, L. (2009) SIRT5 deacetylates carbamoyl phosphate synthetase 1 and regulates the urea cycle. *Cell* **137,** 560–570
27. Kim, S. C., Chen, Y., Mirza, S., Xu, Y., Lee, J., Liu, P., and Zhao, Y. (2006) A clean, more efficient method for in-solution digestion of protein mixtures without detergent or urea. *J. Proteome Res.* **5,** 3446–3452
28. Colaert, N., Helsens, K., Martens, L., Vandekerckhove, J., and Gevaert, K. (2009) Improved visualization of protein consensus sequences by iceLogo. *Nat. Methods* **6,** 786–787
29. Huang da, W., Sherman, B. T., and Lempicki, R. A. (2009) Bioinformatics enrichment tools: paths toward the comprehensive functional analysis of large gene lists. *Nucleic Acids Res.* **37,** 1–13
30. Ashburner, M., Ball, C. A., Blake, J. A., Botstein, D., Butler, H., Cherry, J. M., Davis, A. P., Dolinski, K., Dwight, S. S., Eppig, J. T., Harris, M. A., Hill, D. P., Issel-Tarver, L., Kasarskis, A., Lewis, S., Matese, J. C., Richardson, J. E., Ringwald, M., Rubin, G. M., and Sherlock, G. (2000) Gene ontology: tool for the unification of biology. The Gene Ontology Consortium. *Nat. Genet.* **25,** 25–29
31. Kanehisa, M., and Goto, S. (2000) KEGG: Kyoto encyclopedia of genes and genomes. *Nucleic Acids Res.* **28,** 27–30
32. Jensen, L. J., Kuhn, M., Stark, M., Chaffron, S., Creevey, C., Muller, J., Doerks, T., Julien, P., Roth, A., Simonovic, M., Bork, P., and von Mering, C. (2009) STRING 8—a global view on proteins and their functional interactions in 630 organisms. *Nucleic Acids Res.* **37,** D412–D416
33. Olsen, J. V., Vermeulen, M., Santamaria, A., Kumar, C., Miller, M. L., Jensen, L. J., Gnad, F., Cox, J., Jensen, T. S., Nigg, E. A., Brunak, S., and Mann, M. (2010) Quantitative phosphoproteomics reveals widespread full phosphorylation site occupancy during mitosis. *Sci. Signal.* **3,** ra3
34. Colak, G., Xie, Z., Zhu, A. Y., Dai, L., Lu, Z., Zhang, Y., Wan, X., Chen, Y., Cha, Y. H., Lin, H., Zhao, Y., and Tan, M. (2013) Identification of lysine succinylation substrates and the succinylation regulatory enzyme CobB in *Escherichia coli*. *Mol. Cell. Proteomics* **12,** 3509–3520
35. Salabei, J. K., Gibb, A. A., and Hill, B. G. (2014) Comprehensive measurement of respiratory activity in permeabilized cells using extracellular flux analysis. *Nat. Protoc.* **9,** 421–438
36. Nouws, J., Nijtmans, L., Houten, S. M., van den Brand, M., Huynen, M., Venselaar, H., Hoefs, S., Gloerich, J., Kronick, J., Hutchin, T., Willems, P., Rodenburg, R., Wanders, R., van den Heuvel, L., Smeitink, J., and Vogel, R. O. (2010) Acyl-CoA dehydrogenase 9 is required for the biogenesis of oxidative phosphorylation complex I. *Cell Metab.* **12,** 283–294
37. Wanders, R. J., IJlst, L., van Gennip, A. H., Jakobs, C., de Jager, J. P., Dorland, L., van Sprang, F. J., and Duran, M. (1990) Long-chain 3-hydroxyacyl-CoA dehydrogenase deficiency: identification of a new inborn error of mitochondrial fatty acid β-oxidation. *J. Inher. Metab. Dis.* **13,** 311–314
38. Kridel, S. J., Axelrod, F., Rozenkrantz, N., and Smith, J. W. (2004) Orlistat is a novel inhibitor of fatty acid synthase with antitumor activity. *Cancer Res.* **64,** 2070–2075
39. Zhang, Z., Tan, M., Xie, Z., Dai, L., Chen, Y., and Zhao, Y. (2011) Identification of lysine succinylation as a new post-translational modification. *Nat. Chem. Biol.* **7,** 58–63
40. Kim, S. C., Sprung, R., Chen, Y., Xu, Y., Ball, H., Pei, J., Cheng, T., Kho, Y., Xiao, H., Xiao, L., Grishin, N. V., White, M., Yang, X. J., and Zhao, Y. (2006) Substrate and functional diversity of lysine acetylation revealed by a proteomics survey. *Mol. Cell* **23,** 607–618
41. Choudhary, C., Kumar, C., Gnad, F., Nielsen, M. L., Rehman, M., Walther, T. C., Olsen, J. V., and Mann, M. (2009) Lysine acetylation targets protein complexes and co-regulates major cellular functions. *Science* **325,** 834–840
42. Zhao, S., Xu, W., Jiang, W., Yu, W., Lin, Y., Zhang, T., Yao, J., Zhou, L., Zeng, Y., Li, H., Li, Y., Shi, J., An, W., Hancock, S. M., He, F., Qin, L., Chin, J., Yang, P., Chen, X., Lei, Q., Xiong, Y., and Guan, K. L. (2010) Regulation of cellular metabolism by protein lysine acetylation. *Science* **327,** 1000–1004
43. Chen, Y., Zhao, W., Yang, J. S., Cheng, Z., Luo, H., Lu, Z., Tan, M., Gu, W., and Zhao, Y. (2012) Quantitative acetylome analysis reveals the roles of SIRT1 in regulating diverse substrates and cellular pathways. *Mol. Cell. Proteomics* **11,** 1048–1062
44. Hebert, A. S., Dittenhafer-Reed, K. E., Yu, W., Bailey, D. J., Selen, E. S., Boersma, M. D., Carson, J. J., Tonelli, M., Balloon, A. J., Higbee, A. J., Westphall, M. S., Pagliarini, D. J., Prolla, T. A., Assadi-Porter, F., Roy, S., Denu, J. M., and Coon, J. J. (2013) Calorie restriction and SIRT3 trigger global reprogramming of the mitochondrial protein acetylome. *Mol. Cell* **49,** 186–199
45. Malvagia, S., Papi, L., Morrone, A., Donati, M. A., Ciani, F., Pasquini, E., la Marca, G., Scholte, H. R., Genuardi, M., and Zammarchi, E. (2007) Fatal malonyl CoA decarboxylase deficiency due to maternal uniparental isodisomy of the telomeric end of chromosome 16. *Ann. Hum. Genet.* **71,** 705–712
46. Ostergaard, E. (2008) Disorders caused by deficiency of succinate-CoA ligase. *J. Inher. Metab. Dis.* **31,** 226–229
47. Weinert, B. T., Schölz, C., Wagner, S. A., Iesmantavicius, V., Su, D., Daniel, J. A., and Choudhary, C. (2013) Lysine succinylation is a frequently occurring modification in prokaryotes and eukaryotes and extensively overlaps with acetylation. *Cell Rep.* **4,** 842–851
48. Wild, P., Farhan, H., McEwan, D. G., Wagner, S., Rogov, V. V., Brady, N. R., Richter, B., Korac, J., Waidmann, O., Choudhary, C., Dötsch, V., Bumann, D., and Dikic, I. (2011) Phosphorylation of the autophagy receptor optineurin restricts Salmonella growth. *Science* **333,** 228–233
49. Michishita, E., Park, J. Y., Burneskis, J. M., Barrett, J. C., and Horikawa, I. (2005) Evolutionarily conserved and nonconserved cellular localizations and functions of human SIRT proteins. *Mol. Biol. Cell* **16,** 4623–4635
50. Pagliarini, D. J., Calvo, S. E., Chang, B., Sheth, S. A., Vafai, S. B., Ong, S. E., Walford, G. A., Sugiana, C., Boneh, A., Chen, W. K., Hill, D. E., Vidal, M., Evans, J. G., Thorburn, D. R., Carr, S. A., and Mootha, V. K. (2008) A mitochondrial protein compendium elucidates complex I disease biology. *Cell* **134,** 112–123
51. Mertins, P., Qiao, J. W., Patel, J., Udeshi, N. D., Clauser, K. R., Mani, D. R., Burgess, M. W., Gillette, M. A., Jaffe, J. D., and Carr, S. A. (2013) Integrated proteomic analysis of post-translational modifications by serial enrichment. *Nat. Methods* **10,** 634–637
52. Montgomery, C., Pei, Z., Watkins, P. A., and Miziorko, H. M. (2012) Identification and characterization of an extramitochondrial human 3-hydroxy-3-methylglutaryl-CoA lyase. *J. Biol. Chem.* **287,** 33227–33236
53. Carrasco, P., Menao, S., López-Viñas, E., Santpere, G., Clotet, J., Sierra, A. Y., Gratacós, E., Puisac, B., Gómez-Puertas, P., Hegardt, F. G., Pie, J., and Casals, N. (2007) C-terminal end and aminoacid Lys48 in HMG-CoA lyase are involved in substrate binding and enzyme activity. *Mol. Genet. Metab.* **91,** 120–127
54. McAndrew, R. P., Wang, Y., Mohsen, A. W., He, M., Vockley, J., and Kim, J. J. (2008) Structural basis for substrate fatty acyl chain specificity: crystal structure of human very-long-chain acyl-CoA dehydrogenase. *J. Biol. Chem.* **283,** 9435–9443
55. Wagner, G. R., and Payne, R. M. (2013) Widespread and enzyme-independent N^{ε}-acetylation and N^{ε}-succinylation of proteins in the chemical conditions of the mitochondrial matrix. *J. Biol. Chem.* **288,** 29036–29045
56. Salomons, G. S., Jakobs, C., Pope, L. L., Errami, A., Potter, M., Nowaczyk, M., Olpin, S., Manning, N., Raiman, J. A., Slade, T., Champion, M. P., Peck, D., Gavrilov, D., Hillman, R., Hoganson, G. E., Donaldson, K., Shield, J. P., Ketteridge, D., Wasserstein, M., and Gibson, K. M. (2007) Clinical, enzymatic and molecular characterization of nine new patients with malonyl-coenzyme A decarboxylase deficiency. *J. Inher. Metab. Dis.* **30,** 23–28
57. Houten, S. M., and Wanders, R. J. (2010) A general introduction to the biochemistry of mitochondrial fatty acid β-oxidation. *J. Inher. Metab. Dis.* **33,** 469–477
58. Bennett, M. J., Harthcock, P. A., Boriack, R. L., and Cohen, J. C. (2001) Impaired mitochondrial fatty acid oxidative flux in fibroblasts from a patient with malonyl-CoA decarboxylase deficiency. *Mol. Genet. Metab.* **73,** 276–279
59. de Wit, M. C., de Coo, I. F., Verbeek, E., Schot, R., Schoonderwoerd, G. C., Duran, M., de Klerk, J. B., Huijmans, J. G., Lequin, M. H., Verheijen, F. W., and Mancini, G. M. (2006) Brain abnormalities in a case of malonyl-CoA decarboxylase deficiency. *Mol. Genet. Metab.* **87,** 102–106
60. Nishida, Y., Rardin, M. J., Carrico, C., He, W., Sahu, A. K., Gut, P., Najjar, R., Fitch, M., Hellerstein, M., Gibson, B. W., and Verdin, E. (2015) SIRT5 Regulates both cytosolic and mitochondrial protein malonylation with glycolysis as a major target. *Mol. Cell* **59,** 321–332